

Static axially symmetric Einstein-Yang-Mills-dilaton solutions. II. Black hole solutions

Burkhard Kleihaus and Jutta Kunz

Fachbereich Physik, Universität Oldenburg, Postfach 2503 D-26111 Oldenburg, Germany

(Received 22 December 1997; published 4 May 1998)

We discuss the new class of static axially symmetric black hole solutions obtained recently in Einstein-Yang-Mills and Einstein-Yang-Mills-dilaton theory. These black hole solutions are asymptotically flat and they possess a regular event horizon. The event horizon is almost spherically symmetric with a slight elongation along the symmetry axis. The energy density of the matter fields is angle-dependent at the horizon. The static axially symmetric black hole solutions satisfy a simple relation between mass, dilaton charge, entropy and temperature. The black hole solutions are characterized by two integers, the winding number n and the node number k of the purely magnetic gauge field. With increasing node number the magnetically neutral black hole solutions form sequences tending to limiting solutions with magnetic charge n , corresponding to Einstein-Maxwell-dilaton black hole solutions for finite dilaton coupling constant and to Reissner-Nordström black hole solutions for vanishing dilaton coupling constant. [S0556-2821(98)01312-5]

PACS number(s): 04.20.Jb, 04.40.Nr, 04.70.Bw

I. INTRODUCTION

The “no hair” conjecture for black holes states that black holes are completely characterized by their mass M , their charge Q and their angular momentum J . This conjecture presents a generalization of rigorous results obtained for scalar fields coupled to gravity [1] as well as for Einstein-Maxwell (EM) theory [2]. In EM theory, the unique family of stationary Kerr-Newman black holes with nontrivial values of M , Q , and J contains the stationary Kerr black holes for $Q=0$, the static Reissner-Nordström black holes for $J=0$ and the static Schwarzschild black holes for $J=Q=0$. Notably, the static black hole solutions in EM theory are spherically symmetric, and the stationary black hole solutions are axially symmetric.

In recent years counterexamples to the “no hair” conjecture were established in various theories with non-Abelian fields, including Einstein-Yang-Mills (EYM) theory, Einstein-Yang-Mills-dilaton (EYMD) theory, Einstein-Yang-Mills-Higgs (EYMH) theory, and Einstein-Skyrme (ES) theory [3]. Possessing non-trivial matter fields outside their regular event horizon, these non-Abelian black hole solutions are no more completely determined by their global charges. And they hold more surprises. There are static black hole solutions with only axial symmetry [4], static black hole solutions with only discrete symmetries [5], and there are non-static non-rotational black hole solutions [6]. Unlike the static spherically symmetric [3] and axially symmetric static black hole solutions [4], many of the new types of non-Abelian black hole solutions are only perturbative solutions [5–7].

The static axially symmetric black hole solutions in EYM and EYMD theory [4] have many properties in common with the globally regular static axially symmetric solutions constructed previously [8,9]. Representing generalizations of the static spherically symmetric globally regular and black hole solutions [10–12], these static axially symmetric solutions are characterized by two integers. These are the node number

k of the gauge field functions and the winding number n with respect to the azimuthal angle ϕ . While ϕ covers the full trigonometric circle once, the fields wind n times around. The static spherically symmetric solutions have winding number $n=1$. Winding number $n>1$ leads to axially symmetric solutions.

The static axially symmetric EYM and EYMD black hole solutions [4] are asymptotically flat and possess a regular event horizon. The event horizon of these solutions resides at a surface of constant isotropic radial coordinate. The energy density of the matter fields is not constant at the horizon but angle-dependent. Outside their regular event horizon, the static axially symmetric black hole solutions possess non-trivial magnetic gauge field configurations, but they carry no global magnetic charge. For fixed winding number n and increasing node number k the solutions form sequences, tending to limiting solutions. These limiting solutions are spherically symmetric and Abelian, representing Einstein-Maxwell-dilaton (EMD) [13] and Reissner-Nordström (RN) black hole solutions for EYMD and EYM theory, respectively [8,4,9], which carry magnetic charge n .

Having given a brief account of the properties of these static axially symmetric black hole solutions in [4], we here present these solutions in detail. The paper thus represents the second paper of our sequel on static axially symmetric EYMD solutions, following [9], where a detailed presentation of the globally regular solutions was given. In Sec. II of this paper we recall the action, we present the static axially symmetric ansatz in isotropic coordinates and we discuss the boundary conditions. Introducing temperature and entropy of the black hole solutions, we derive a relation between these thermodynamic quantities and the mass and the dilaton charge. In Sec. III we recall the static spherically symmetric black hole solutions and present them in isotropic coordinates. In Sec. IV we present the static axially symmetric black hole solutions, discuss their properties, and analyze the properties of their event horizon. We show that the sequences of neutral non-Abelian solutions tend to limiting

charged Abelian solutions. We present our conclusions in Sec. V. In Appendix A we present the expansion of the functions at the horizon, and we show that the Kretschmann scalar is finite there. In Appendix B we discuss the final choice of functions for the numerical integration.

II. STATIC AXIALLY SYMMETRIC ANSATZ

We consider the SU(2) Einstein-Yang-Mills-dilaton action

$$S = \int \left(\frac{R}{16\pi G} + L_M \right) \sqrt{-g} d^4x \quad (1)$$

with the matter Lagrangian

$$L_M = -\frac{1}{2} \partial_\mu \Phi \partial^\mu \Phi - e^{2\kappa\Phi} \frac{1}{2} \text{Tr}(F_{\mu\nu} F^{\mu\nu}), \quad (2)$$

the field strength tensor

$$F_{\mu\nu} = \partial_\mu A_\nu - \partial_\nu A_\mu + ie[A_\mu, A_\nu], \quad (3)$$

the gauge field

$$A_\mu = \frac{1}{2} \tau^a A_\mu^a, \quad (4)$$

the dilaton field Φ , and the Yang-Mills and dilaton coupling constants e and κ , respectively.

Variation of the action (1) with respect to the metric $g^{\mu\nu}$ leads to the Einstein equations, variation with respect to the gauge field A_μ and the dilaton field Φ leads to the matter field equations [9].

A. Static axially symmetric ansatz

As for the globally regular static axially symmetric solutions [8,9], we adopt isotropic coordinates to construct the static axially symmetric black hole solutions. In terms of the coordinates r , θ and ϕ the isotropic metric reads

$$ds^2 = -f dt^2 + \frac{m}{f} dr^2 + \frac{mr^2}{f} d\theta^2 + \frac{lr^2 \sin^2 \theta}{f} d\phi^2, \quad (5)$$

where the metric functions f , m and l are only functions of the coordinates r and θ . Regularity on the z -axis ($z = r \cos \theta$) requires [14]

$$m|_{\theta=0} = l|_{\theta=0}. \quad (6)$$

Again, we consider a purely magnetic gauge field, $A_0 = 0$, and choose for the gauge field the ansatz [15–17,8,4,9]

$$A_\mu dx^\mu = \frac{1}{2er} \{ \tau_\phi^n [H_1 dr + (1 - H_2) r d\theta] - n [\tau_r^n H_3 + \tau_\theta^n (1 - H_4)] r \sin \theta d\phi \}, \quad (7)$$

where the symbols τ_r^n , τ_θ^n and τ_ϕ^n denote the dot products of the Cartesian vector of Pauli matrices, $\vec{\tau} = (\tau_x, \tau_y, \tau_z)$, with the spatial unit vectors

$$\begin{aligned} \vec{e}_r^n &= (\sin \theta \cos n\phi, \sin \theta \sin n\phi, \cos \theta), \\ \vec{e}_\theta^n &= (\cos \theta \cos n\phi, \cos \theta \sin n\phi, -\sin \theta), \\ \vec{e}_\phi^n &= (-\sin n\phi, \cos n\phi, 0), \end{aligned} \quad (8)$$

respectively. Since the fields wind n times around, while the azimuthal angle ϕ covers the full trigonometric circle once, we refer to the integer n as the winding number of the solutions. The four gauge field functions H_i and the dilaton function Φ depend only on the coordinates r and θ . The spherically symmetric ansatz [12] is recovered for $n=1$ and $H_1 = H_3 = 0$, $H_2 = H_4 = w(r)$ and $\Phi = \Phi(r)$.

The ansatz (7) is axially symmetric in the sense, that a rotation around the z -axis can be compensated by a gauge rotation. Besides being axially symmetric the ansatz respects the discrete mirror symmetry $M_{xz} \otimes C$, where the first factor represents reflection through the xz -plane and the second factor denotes charge conjugation [18,16,19].

The ansatz is form-invariant under the Abelian gauge transformation [18,16,17]

$$U = \exp \left(\frac{i}{2} \tau_\phi^n \Gamma(r, \theta) \right). \quad (9)$$

The functions H_1 and H_2 transform inhomogeneously under this gauge transformation

$$\begin{aligned} H_1 &\rightarrow H_1 - r \partial_r \Gamma, \\ H_2 &\rightarrow H_2 + \partial_\theta \Gamma, \end{aligned} \quad (10)$$

like a two-dimensional gauge field. The functions H_3 and H_4 combine to form a scalar doublet, $(H_3 + \text{ctg} \theta, H_4)$. We choose the same gauge condition as previously [18,16,17,8,4,9]:

$$r \partial_r H_1 - \partial_\theta H_2 = 0. \quad (11)$$

With the ansatz (5)–(7) and the gauge condition (11) we obtain the set of EYMD field equations, given in [9].

The energy density of the matter fields $\epsilon = -T_0^0 = -L_M$ reads

$$\begin{aligned} -T_0^0 &= \frac{f}{2m} \left[(\partial_r \Phi)^2 + \frac{1}{r^2} (\partial_\theta \Phi)^2 \right] + e^{2\kappa\Phi} \frac{f^2}{2e^2 r^4 m} \left\{ \frac{1}{m} (r \partial_r H_2 + \partial_\theta H_1)^2 + \frac{n^2}{l} \{ (r \partial_r H_3 - H_1 H_4)^2 + [r \partial_r H_4 + H_1 (H_3 + \text{ctg} \theta)]^2 \right. \\ &\quad \left. + (\partial_\theta H_3 - 1 + \text{ctg} \theta H_3 + H_2 H_4)^2 + [\partial_\theta H_4 + \text{ctg} \theta (H_4 - H_2) - H_2 H_3]^2 \right\}. \end{aligned} \quad (12)$$

Here the first gauge field term derives from $F_{r\theta}$, the second and third derive from $F_{r\phi}$ and the fourth and fifth from $F_{\theta\phi}$. As seen from Eq. (12), regularity on the z -axis requires

$$H_2|_{\theta=0} = H_4|_{\theta=0}. \quad (13)$$

B. Boundary conditions

To obtain asymptotically flat solutions with a regular event horizon and with the proper symmetries, we must impose the appropriate boundary conditions, the boundaries being the horizon and radial infinity, the z -axis and, because of parity reflection symmetry, the ρ -axis. The presence of a regular event horizon is the essential new feature of the static axially symmetric black hole solutions, as compared to the globally regular solutions. We therefore begin with a detailed discussion of the boundary conditions at the horizon. The boundary conditions at infinity and along the ρ - and the z -axis agree with those of the globally regular solutions [8,9]. They are only briefly recalled for completeness.

Boundary conditions at the horizon. The event horizon of the static black hole solutions is characterized by $g_{tt} = -f = 0$, g_{rr} is finite at the horizon in isotropic coordinates. We impose that the horizon of the black hole solutions resides at a surface of constant r , $r = r_H$ [20]. This ansatz for the event horizon is justified *a posteriori*, since it leads to consistent solutions, possessing a regular event horizon.

Requiring the horizon to be regular, we obtain the boundary conditions at the horizon $r = r_H$. The metric functions must satisfy

$$f|_{r=r_H} = m|_{r=r_H} = l|_{r=r_H} = 0, \quad (14)$$

and the dilaton function

$$\partial_r \Phi|_{r=r_H} = 0. \quad (15)$$

The conditions for the gauge field functions are

$$\begin{aligned} (\partial_\theta H_1 + r \partial_r H_2)|_{r=r_H} &= 0, \\ (r \partial_r H_3 - H_1 H_4)|_{r=r_H} &= 0, \\ [r \partial_r H_4 + H_1(H_3 + \text{ctg } \theta)]|_{r=r_H} &= 0, \end{aligned} \quad (16)$$

which imply, $F_{r\theta} = 0$ and $F_{r\phi} = 0$, respectively.

Thus the equations of motion yield only three boundary conditions for the four gauge field functions H_i ; one gauge field boundary condition is left indeterminate. However, for the black hole solutions precisely one free boundary condition at the horizon is necessary to completely fix the gauge. The reason is, that in contrast to the case of the globally regular solutions [8], for the black hole solutions the gauge condition (11) still allows non-trivial gauge transformations satisfying

$$r^2 \partial_r^2 \Gamma + r \partial_r \Gamma + \partial_\theta^2 \Gamma = 0. \quad (17)$$

To fix the gauge, we have implemented various gauge conditions at the horizon, such as

$$(\partial_r H_1)|_{r=r_H} = 0, \quad (18)$$

or

$$(\partial_\theta H_1)|_{r=r_H} = 0, \quad (19)$$

obtaining the same results for the gauge invariant quantities.

The expansions of the functions at the regular horizon are given in Appendix A 1.

Boundary conditions at infinity. At infinity ($r = \infty$) we require the boundary conditions [8,4,9]

$$f|_{r=\infty} = m|_{r=\infty} = l|_{r=\infty} = 1, \quad (20)$$

$$\Phi|_{r=\infty} = 0, \quad (21)$$

[since any finite value of the dilaton field at infinity can be transformed to zero via $\Phi \rightarrow \Phi - \Phi(\infty)$, $r \rightarrow r e^{-\kappa \Phi(\infty)}$] and

$$H_2|_{r=\infty} = H_4|_{r=\infty} = \pm 1, \quad H_1|_{r=\infty} = H_3|_{r=\infty} = 0, \quad (22)$$

to obtain magnetically neutral solutions. The expansion of the functions at infinity is given in [9].

The node number k is defined by the number of nodes of the gauge field functions H_2 and H_4 [9]. Because of the symmetry with respect to the transformation $H_i \rightarrow -H_i$, we can choose these gauge field functions to be positive at the horizon. Solutions with an even number of nodes then have $H_2(\infty) = H_4(\infty) = 1$, whereas solutions with an odd number of nodes have $H_2(\infty) = H_4(\infty) = -1$.

Boundary conditions along the axes. The symmetries determine the boundary conditions along the ρ -axis and the z -axis [8,4,9]:

$$\begin{aligned} \partial_\theta f|_{\theta=0} &= \partial_\theta m|_{\theta=0} = \partial_\theta l|_{\theta=0} = 0, \\ \partial_\theta f|_{\theta=\pi/2} &= \partial_\theta m|_{\theta=\pi/2} = \partial_\theta l|_{\theta=\pi/2} = 0, \\ \partial_\theta \Phi|_{\theta=0} &= 0, \\ \partial_\theta \Phi|_{\theta=\pi/2} &= 0, \end{aligned} \quad (23)$$

and

$$\begin{aligned} H_1|_{\theta=0} &= H_3|_{\theta=0} = 0, \\ \partial_\theta H_2|_{\theta=0} &= \partial_\theta H_4|_{\theta=0} = 0, \\ H_1|_{\theta=\pi/2} &= H_3|_{\theta=\pi/2} = 0, \\ \partial_\theta H_2|_{\theta=\pi/2} &= \partial_\theta H_4|_{\theta=\pi/2} = 0. \end{aligned} \quad (25)$$

In addition, regularity on the z -axis requires condition (6) for the metric functions to be satisfied (see Appendix B) and condition (13) for the gauge field functions. The expansion of the functions on the positive z -axis is given in [9].

C. Dimensionless quantities

As previously, we introduce the dimensionless coordinate x ,

$$x = \frac{e}{\sqrt{4\pi G}} r, \quad (26)$$

the dimensionless dilaton function φ ,

$$\varphi = \sqrt{4\pi G} \Phi, \quad (27)$$

and the dimensionless dilaton coupling constant γ ,

$$\gamma = \frac{1}{\sqrt{4\pi G}} \kappa. \quad (28)$$

The dilaton coupling constant γ represents a parameter; for $\gamma=1$ contact with the low energy effective action of string theory is made, whereas in the limit $\gamma \rightarrow 0$ the dilaton decouples and EYM theory is obtained.

The dimensionless mass μ is related to the mass M via

$$\mu = \frac{eG}{\sqrt{4\pi G}} M. \quad (29)$$

D. Mass, temperature and entropy

The mass M of the black hole solutions can be obtained directly from the total energy-momentum “tensor” $\tau^{\mu\nu}$ of matter and gravitation [21]

$$M = \int \tau^{00} d^3r. \quad (30)$$

As shown in [9], the dimensionless mass μ is then determined by the derivative of the metric function f at infinity

$$\mu = \frac{1}{2} \lim_{x \rightarrow \infty} x^2 \partial_x f. \quad (31)$$

The zeroth law of black hole physics states that the surface gravity κ_{sg} is constant at the horizon of the black hole solutions; here [22,5]

$$\kappa_{\text{sg}}^2 = -(1/4) g^{tt} g^{ij} (\partial_i g_{tt}) (\partial_j g_{tt}). \quad (32)$$

To evaluate κ_{sg} , we need to consider the metric functions at the horizon. Expanding the equations in the vicinity of the horizon in powers of the dimensionless coordinate $(x - x_H)/x_H$, we observe that the metric functions are quadratic in $x - x_H$,

$$f(x, \theta) = f_2(\theta) \left(\frac{x - x_H}{x_H} \right)^2 \left(1 - \frac{x - x_H}{x_H} \right) + O \left(\frac{x - x_H}{x_H} \right)^4, \quad (33)$$

$$m(x, \theta) = m_2(\theta) \left(\frac{x - x_H}{x_H} \right)^2 \left(1 - 3 \frac{x - x_H}{x_H} \right) + O \left(\frac{x - x_H}{x_H} \right)^4, \quad (34)$$

and likewise Eq. (34) for $l(x, \theta)$ (see Appendix A 1). Since the temperature T is proportional to the surface gravity κ_{sg} [22],

$$T = \kappa_{\text{sg}} / (2\pi), \quad (35)$$

we obtain, for the dimensionless temperature,

$$T = \frac{f_2(\theta)}{2\pi x_H \sqrt{m_2(\theta)}}. \quad (36)$$

To show that the temperature T of the static axially symmetric black hole solutions is indeed constant at the horizon, we employ the expansion of the metric functions (33) and (34) in the $r\theta$ component of the Einstein equations at the horizon. This yields the crucial relation between the expansion coefficients $f_2(\theta)$ and $m_2(\theta)$:

$$0 = \frac{\partial_\theta m_2}{m_2} - 2 \frac{\partial_\theta f_2}{f_2}. \quad (37)$$

The dimensionless area A of the event horizon of the black hole solutions is given by

$$A = 2\pi \int_0^\pi d\theta \sin \theta \frac{\sqrt{l_2 m_2}}{f_2} x_H^2. \quad (38)$$

The entropy S is proportional to the area A [22],

$$S = \frac{A}{4}, \quad (39)$$

leading to the dimensionless product

$$TS = \frac{x_H}{4} \int_0^\pi d\theta \sin \theta \sqrt{l_2}. \quad (40)$$

Having defined temperature and entropy, we now derive a second expression for the mass [22]. As shown before [9], the equations of motion yield

$$\frac{1}{8\pi G} \partial_\mu (\sqrt{-g} \partial^\mu \ln f) = -\sqrt{-g} (2T_0^0 - T_\mu^\mu). \quad (41)$$

Integrating both sides over r , θ and ϕ from the horizon to infinity, we obtain

$$\begin{aligned} & \frac{1}{4G} \int_0^\pi d\theta \sin \theta \left[r^2 \sqrt{l} \frac{\partial_r f}{f} \right] \Big|_{r_H}^\infty \\ &= - \int_0^{2\pi} \int_0^\pi \int_{r_H}^\infty d\phi d\theta dr \sqrt{-g} (2T_0^0 - T_\mu^\mu) = M_o. \end{aligned} \quad (42)$$

Changing to dimensionless coordinates, we express the left-hand side (LHS) with help of the dimensionless mass μ and the product of temperature and entropy TS , obtaining

$$\mu = \mu_o + 2TS, \quad (43)$$

with $\mu_o = (e/\sqrt{4\pi G}) G M_o$, in agreement with the general mass formula for static black hole solutions [22].

Considering the dilaton field equation in the form [9]

$$\frac{1}{\kappa} \partial_\mu (\sqrt{-g} \partial^\mu \Phi) = \frac{1}{8\pi G} \partial_\mu (\sqrt{-g} \partial^\mu \ln f), \quad (44)$$

it is straightforward to derive a relation between mass the μ and the dilaton charge D :

$$D = \lim_{x \rightarrow \infty} x^2 \partial_x \varphi. \quad (45)$$

We replace the left-hand side (LHS) of Eq. (41) by the LHS of Eq. (44) and integrate as above. Recalling the boundary condition $\partial_r \Phi|_{r=r_H} = 0$ and changing to dimensionless coordinates, we obtain

$$D = \gamma \mu_o = \gamma(\mu - 2TS), \quad (46)$$

where the second equality follows from Eq. (43).

Previously we obtained for static spherically symmetric black holes the relation [23]

$$D = \gamma \left(\mu - \frac{\mu_S}{T_S} T \right), \quad (47)$$

where $\mu_S = \tilde{x}_H/2$ and $T_S = 1/(4\pi\tilde{x}_H)$ represent the Schwarzschild mass and the Schwarzschild temperature of a black hole with horizon \tilde{x}_H in Schwarzschild-like coordinates. This relation represents a special case of the more general relation (46), since for a spherical black hole $A = 4\pi\tilde{x}_H^2$.

III. SPHERICALLY SYMMETRIC SOLUTIONS

The static spherically symmetric EYM and EYMD solutions were obtained previously in Schwarzschild-like coordinates with metric [10,12,23]

$$ds^2 = -A^2 N dt^2 + \frac{1}{N} d\tilde{r}^2 + \tilde{r}^2 (d\theta^2 + \sin^2 \theta d\phi^2) \quad (48)$$

and metric functions $A(\tilde{r})$ and $N(\tilde{r})$,

$$N(\tilde{r}) = 1 - \frac{2\tilde{m}(\tilde{r})}{\tilde{r}}. \quad (49)$$

We here briefly present the spherical solutions in isotropic coordinates. We exhibit the coordinate transformation between the radial coordinates r and \tilde{r} , and we discuss the limiting solutions.

A. Coordinate transformation

The static spherically symmetric isotropic metric reads

$$ds^2 = -f dt^2 + \frac{m}{f} [dr^2 + r^2 (d\theta^2 + \sin^2 \theta d\phi^2)]. \quad (50)$$

The coordinates r and \tilde{r} are related by

$$\frac{dr}{r} = \frac{1}{\sqrt{N(\tilde{r})}} \frac{d\tilde{r}}{\tilde{r}}. \quad (51)$$

Changing to dimensionless coordinates x and \tilde{x} , the coordinate function $x(\tilde{x})$ must be obtained numerically from Eq. (51), since the function $N(\tilde{x})$ of the non-Abelian solutions is only known numerically. To avoid the divergence of $1/N(\tilde{x})$ at the horizon in the numerical integration, we introduce the function $\Delta(\tilde{x})$:

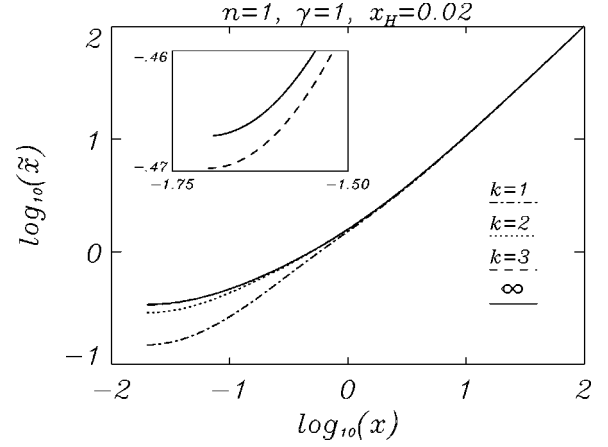


FIG. 1. The coordinate transformation between the isotropic coordinate x and the Schwarzschild-like coordinate \tilde{x} is shown for the static spherically symmetric solutions ($n=1$) of EYMD theory with $\gamma=1$ and $k=1-3$. Also shown is the coordinate transformation for the limiting EMD solution.

$$\Delta(\tilde{x}) = \frac{1}{\sqrt{N(\tilde{x})}} - \frac{1}{c\sqrt{N_S(\tilde{x})}}, \quad (52)$$

where

$$c^2 = \tilde{x} \frac{dN}{d\tilde{x}} \bigg|_{\tilde{x}=\tilde{x}_H} \quad (53)$$

and N_S is the Schwarzschild metric function

$$N_S(\tilde{x}) = 1 - \frac{\tilde{x}_H}{\tilde{x}}. \quad (54)$$

After replacing on the RHS of Eq. (51) $1/\sqrt{N}$ by $1/c\sqrt{N_S} + \Delta$, we integrate the first term analytically and the finite Δ -term numerically. This yields the coordinate transformation

$$x = \left(\frac{2\sqrt{\tilde{x}(\tilde{x} - \tilde{x}_H)} + 2\tilde{x} - \tilde{x}_H}{4} \right)^{1/c} \exp \left[\int_{\tilde{x}_H}^{\tilde{x}} \frac{\Delta(\tilde{x}')}{\tilde{x}'} d\tilde{x}' \right], \quad (55)$$

where

$$x_H = \left(\frac{\tilde{x}_H}{4} \right)^{1/c} \quad (56)$$

is determined by the asymptotic requirement, $x/\tilde{x} \rightarrow 1$. For the Schwarzschild solution $c=1$, and $x_H = \tilde{x}_H/4$.

Figure 1 demonstrates the coordinate transformation for the static spherically symmetric EYMD solutions with $x_H=0.02$, $\gamma=1$ and $k=1-4$. Figures 2(a), 2(b) show the metric functions f and m , and Figs. 3(a), 3(b) show the gauge field function w and the dilaton function φ .

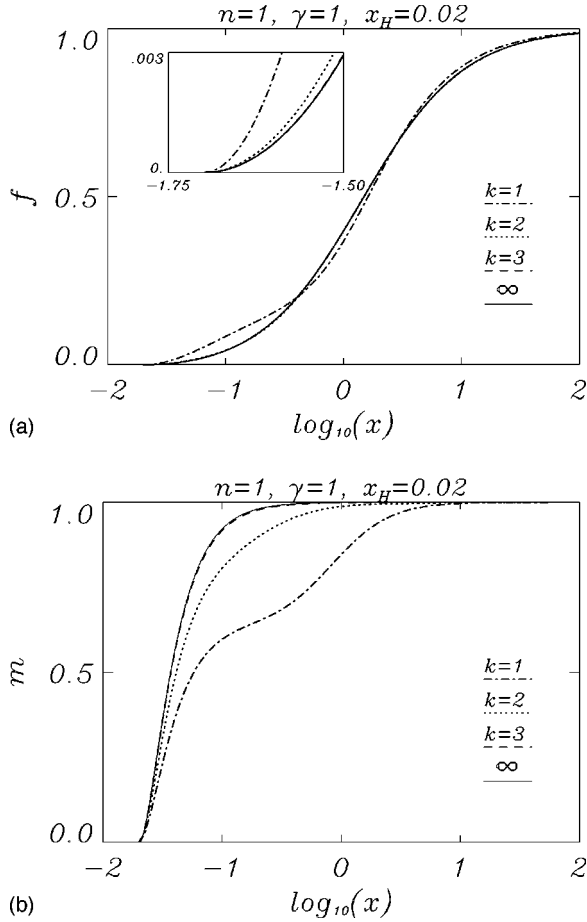


FIG. 2. (a) The metric function f is shown for the static spherically symmetric solutions ($n=1$) of EYMD theory with $\gamma=1$ and $k=1-3$. Also shown is the metric function of the limiting EMD solution. (b) Same as (a) for the metric function m .

Figure 4 demonstrates the coordinate transformation for the static spherically symmetric EYM solutions with $x_H=0.02$ and $k=1-4$. Figs. 5(a), 5(b) show the metric functions f and m .

B. Limiting solutions

For fixed dilaton coupling constant and horizon, the sequences of neutral static spherically symmetric EYMD black hole solutions converge to limiting solutions [23]. These limiting solutions are EMD black hole solutions [13] with the same dilaton coupling constant, the same horizon and charge $P=1$ [23].

We now consider the limiting EMD solution for $\gamma=1$ and a general charge P . Defining [13]

$$X_+ = \sqrt{\tilde{x}_H^2 + 2P^2}, \quad X_- = \frac{2P^2}{X_+}, \quad (57)$$

and

$$X = \frac{X_- + \sqrt{4\tilde{x}^2 + X_-^2}}{2}, \quad (58)$$

i.e., $X_H = X_+$, the coordinate transformation for the limiting EMD solution reads

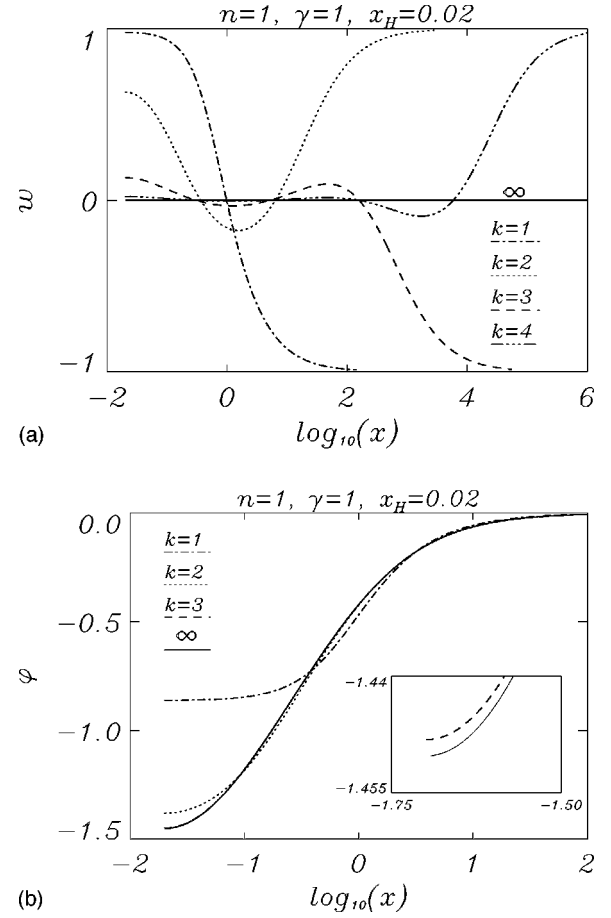


FIG. 3. (a) Same as Fig. 2(a) for the gauge field function w , for $k=1-4$. (b) Same as Fig. 2(a) for the dilaton function ϕ .

$$x = \frac{2\sqrt{(X-X_-)(X-X_+)} + 2X - (X_- + X_+)}{4}, \quad (59)$$

with

$$x_H = \frac{X_+ - X_-}{4}. \quad (60)$$

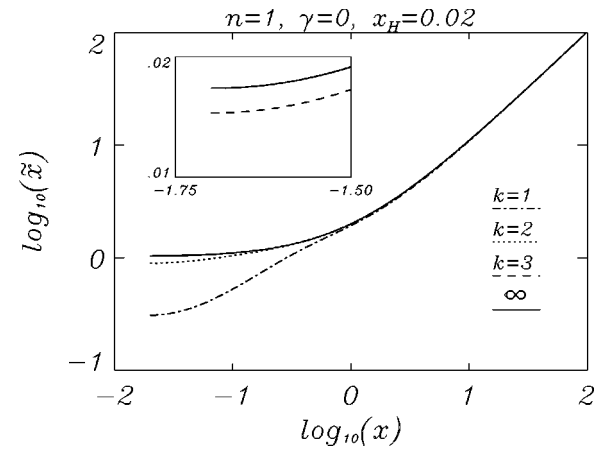


FIG. 4. The coordinate transformation between the isotropic coordinate x and the Schwarzschild-like coordinate \tilde{x} is shown for the static spherically symmetric solutions ($n=1$) of EYM theory with $k=1-3$. Also shown is the coordinate transformation for the limiting RN solution.

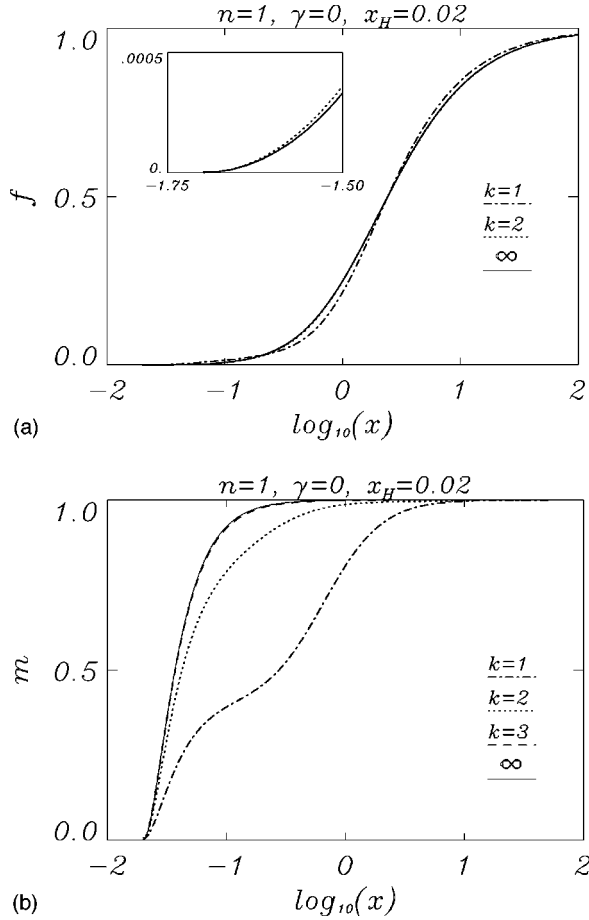


FIG. 5. (a) The metric function f is shown for the static spherically symmetric solutions ($n=1$) of EYM theory with $k=1-2$. Also shown is the metric function of the limiting RN solution. (b) Same as (a) for the metric function m for $k=1-3$.

The metric functions of the limiting solution read in isotropic coordinates

$$f_\infty = \frac{(1 - x_H/x)^2}{[1 + 2(x_H/x)\sqrt{1 + 1/2(P/x_H)^2} + (x_H/x)^2]} \quad (61)$$

and

$$m_\infty = \left[1 - \left(\frac{x_H}{x} \right)^2 \right]^2. \quad (62)$$

The dilaton function of the limiting solution reads

$$e^{2\varphi_\infty} = \frac{(1 + x_H/x)^2}{[1 + 2(x_H/x)\sqrt{1 + 1/2(P/x_H)^2} + (x_H/x)^2]}. \quad (63)$$

The gauge field function of the limiting solution is trivial, $w_\infty = 0$. For $P=1$ and $x_H=0.02$ the coordinate transformation for the limiting solution is shown in Fig. 1, the metric functions of the limiting solution are shown in Figs. 2 and the dilaton function in Fig. 3. For the horizon $x_H=0.02$ the convergence is rapid. The solution with $k=3$ is already very close to the limiting solution, and the solution with $k=4$ is almost indistinguishable, for all functions except for the gauge field function w . This function approaches its limiting function $w_\infty = 0$ non-uniformly, since the boundary condi-

tions require $w(\infty) \neq 0$. A detailed discussion on the convergence of these solutions is given in [23].

We now turn to the limiting solutions of the sequences of static spherically symmetric EYM black hole solutions. In Schwarzschild-like coordinates, the limiting solution of the sequence with fixed horizon \tilde{x}_H , is a RN solution with the same horizon and with charge $P=1$, if $\tilde{x}_H > 1$ [24,23]. If $\tilde{x}_H < 1$, the limiting solution consists of two parts, an exterior part covering the interval $1 < \tilde{x} < \infty$, which represents the exterior of an extremal RN solution with mass $\mu=1$, horizon $\tilde{x}_H=1$ and charge $P=1$, and an oscillating interior part covering the interval $\tilde{x}_H < \tilde{x} < 1$ [24,23,25]. In isotropic coordinates with fixed horizon x_H , the limiting solution corresponds to the exterior of a RN solution with the same horizon and with charge $P=1$.

The coordinate transformation for the limiting RN solution reads

$$x = \frac{\sqrt{\tilde{x}^2 - 2\mu\tilde{x} + P^2} + \tilde{x} - \mu}{2} \quad (64)$$

with

$$\mu = \frac{\tilde{x}_H^2 + P^2}{2\tilde{x}_H}. \quad (65)$$

The metric functions are given by

$$f_\infty = \frac{[1 - (x_H/x)^2]^2}{[1 + 2(x_H/x)\sqrt{1 + 1/4(P/x_H)^2} + (x_H/x)^2]^2} \quad (66)$$

and

$$m_\infty = \left[1 - \left(\frac{x_H}{x} \right)^2 \right]^2, \quad (67)$$

i.e., m_∞ is identical for the EMD and RN solutions. Again, the gauge field function of the limiting solution is trivial, $w_\infty = 0$. For $P=1$ and $x_H=0.02$ the coordinate transformation of the limiting solution is shown in Fig. 4 and the metric functions in Figs. 5.

C. Limit $x_H \rightarrow 0$

Let us now consider the limit $x_H \rightarrow 0$ for the black hole solutions. In this limit the solutions tend towards the corresponding globally regular solutions [11,12,23]. For several quantities of interest, however, the limit $x_H \rightarrow 0$ is not smooth. For instance, the energy density of the matter fields of the black hole solutions approaches the energy density of the globally regular solutions with a discontinuity at the origin. The reason is that the magnetic field of the black hole solutions is purely radial at the horizon

$$\vec{B} = B_r \vec{e}_r, \quad (68)$$

with $B_r = F_{\theta\phi}$, because the boundary conditions (16) require

$$B_\theta = 0, \quad B_\phi = 0, \quad (69)$$

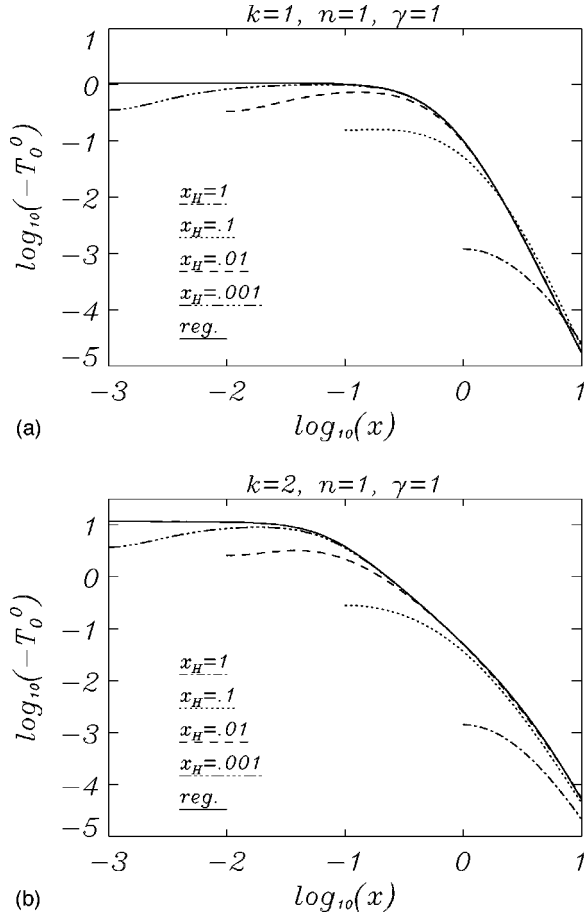


FIG. 6. (a) The energy density $\epsilon = -T_0^0$ is shown for the static spherically symmetric black hole solutions ($n=1$) of EYMD theory with $\gamma=1$ and $k=1$ and the horizon radii $x_H=1, 0.1, 0.01$ and 0.001 , as well as for the corresponding globally regular solution. (b) Same as (a) for $k=2$.

with $B_\theta = -F_{r\phi}$ and $B_\phi = F_{r\theta}$, whereas the magnetic field of the globally regular solutions has non-vanishing B_θ at the origin. We demonstrate this discontinuous behavior of the energy density of the matter fields in Figs. 6(a), 6(b) for the EYMD ($\gamma=1$) solutions with $k=1$ and 2 and $x_H = 0.001, 0.01, 0.1$ and 1 .

We finally consider the Kretschmann scalar K ,

$$K = R^{\mu\nu\alpha\beta} R_{\mu\nu\alpha\beta}. \quad (70)$$

An analytical expression for K is given in Appendix A 2. We show K in Fig. 7 for the same set of EYMD solutions. Again, the limit $x_H \rightarrow 0$ is not smooth. However, as required for a regular horizon, K is finite at the horizon for finite x_H .

IV. AXIALLY SYMMETRIC SOLUTIONS

Subject to the above boundary conditions, we solve the equations for the static axially symmetric black hole solutions numerically. We employ the same numerical algorithm [26] as for the static axially symmetric globally regular solutions [8,4,9]. To map spatial infinity to the finite value $\bar{x} = 1$, we here employ the radial coordinate

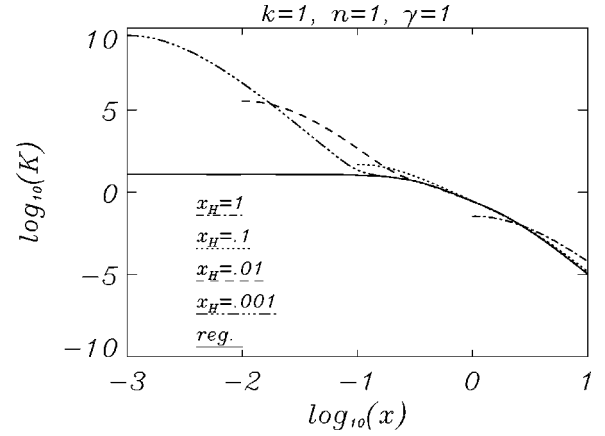


FIG. 7. The Kretschmann scalar is shown for the static spherically symmetric black hole solutions ($n=1$) of EYMD theory with $\gamma=1$ and $k=1$ and the horizon radii $x_H=1, 0.1, 0.01$ and 0.001 , as well as for the corresponding globally regular solution.

$$\bar{x} = 1 - \frac{x_H}{x}. \quad (71)$$

The equations are then discretized on a non-equidistant grid in \bar{x} and θ , where typical grids used have sizes 150×30 , covering the integration region $0 \leq \bar{x} \leq 1$, $0 \leq \theta \leq \pi/2$. The numerical error for the functions is estimated to be on the order of 10^{-3} .

The solutions depend on two continuous parameters, the “isotropic radius” x_H of the horizon and the dilaton coupling constant γ , as well as on two integers, the winding number n and the node number k .

A. Energy density and horizon

We begin our discussion of the static axially symmetric black hole solutions by considering the energy density of the matter fields. As an example we show in Figs. 8 the energy density of the matter fields for the black hole solution with $x_H=1, \gamma=1, n=2$ and $k=1$. Figure 8(a) shows a three-dimensional plot of the energy density as a function of the coordinates $\rho = x \sin \theta$ and $z = x \cos \theta$ together with a contour plot, and Figs. 8(b)–8(e) show surfaces of constant energy density. For small values of ϵ the energy density appears ellipsoidal, being flatter at the poles than in the equatorial plane. With increasing values of ϵ a toruslike shape appears with two additional ellipsoids covering the poles. The ellipsoids covering the poles persist up to the largest values of the energy density, showing that the maximum of the energy density resides at the poles. Furthermore these black hole solutions have the remarkable property, that the energy density is not constant at the horizon but angle-dependent.

The static axially symmetric black hole solutions are self-consistent solutions arising from the interplay of gravity with the non-Abelian gauge fields. In isotropic coordinates the horizon of the static axially symmetric black hole solutions resides at a surface of constant radial coordinate x , $x = x_H$. Since the energy density of the matter fields of the static axially symmetric black hole solutions is angle-dependent at the horizon, this suggests that the horizon is deformed. We

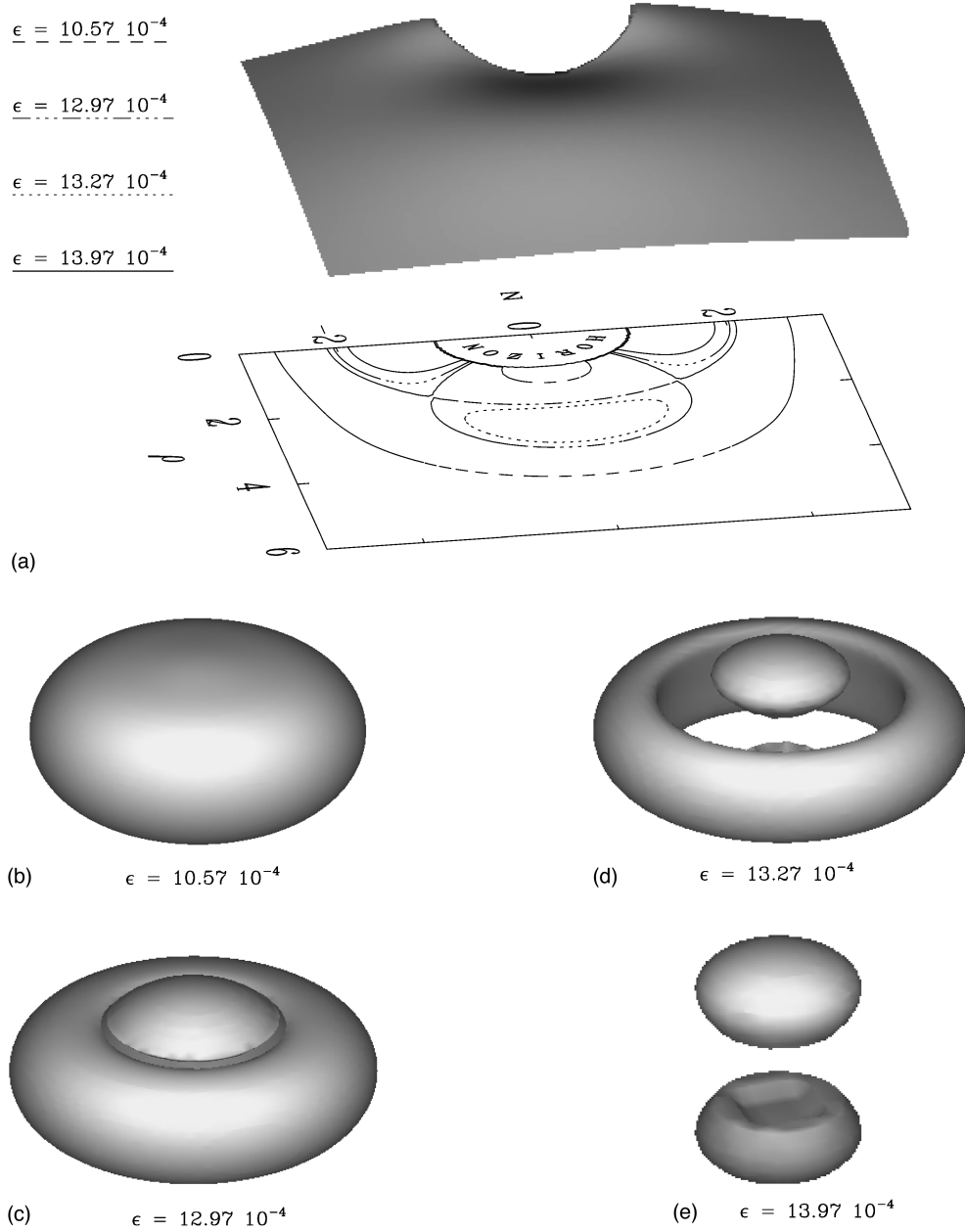


FIG. 8. (a) The energy density $\epsilon = -T_0^0$ is shown for the static axially symmetric black hole solution of EYMD theory with $\gamma=1$, $n=2$ and $k=1$ and the horizon radius $x_H=1$ in a three-dimensional plot and a contour plot with axes ρ and z . (b)–(e) Surfaces of constant energy density $\epsilon = -T_0^0$ are shown for the solution of (a).

therefore measure the circumference of the horizon along the equator, L_e ,

$$L_e = \int_0^{2\pi} d\phi \sqrt{\frac{l}{f}} x \sin \theta \Big|_{x=x_H, \theta=\pi/2} = 2\pi x_H \sqrt{\frac{l_2}{f_2}} \Big|_{\theta=\pi/2}, \quad (72)$$

and the circumference of the horizon along the poles, L_p ,

$$L_p = 2 \int_0^\pi d\theta \sqrt{\frac{m}{f}} x \Big|_{x=x_H, \phi=\text{const}} = 2x_H \int_0^\pi d\theta \sqrt{\frac{m_2(\theta)}{f_2(\theta)}}. \quad (73)$$

A spherical horizon would require $L_e = L_p$. For the static axially symmetric black hole solutions we observe, however,

$$L_p > L_e. \quad (74)$$

Thus the horizon itself possesses only axial symmetry. The deviation from spherical symmetry is small, though. For instance for the solution of Figs. 8 we find $L_e/L_p = 0.998$.

B. x_H dependence of the solutions

Let us now study the dependence of the static axially symmetric solutions on the isotropic black hole horizon radius x_H . To be specific, we consider black hole solutions with $\gamma=1$, $n=2$ and $k=1$, the parameters also employed in

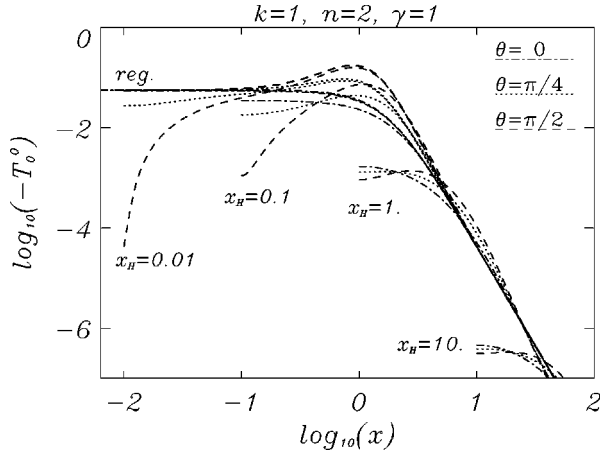


FIG. 9. The energy density $\epsilon = -T_0^0$ is shown as a function of the dimensionless coordinate x for the angles $\theta=0$, $\theta=\pi/4$ and $\theta=\pi/2$ for the EYMD black hole solutions with $\gamma=1$, winding number $n=2$, node number $k=1$ and horizon radii $x_H=0.01$, $x_H=0.1$, $x_H=1$, and $x_H=10$, as well as for the corresponding globally regular solution.

the solution shown in Figs. 8. In Fig. 9 the energy density of the matter fields is shown for several black hole solutions, with values of the isotropic black hole horizon radius $x_H=0.01$, 0.1, 1 and 10, as well as for the globally regular solution. As noted above, for larger values of x_H the global maximum of the energy density of the black hole solutions resides on the z -axis at the horizon, while a local maximum is located on the ρ -axis away from the horizon. With decreasing x_H , the maximum on the ρ -axis away from the horizon increases and becomes the global maximum, while the maximum on the z -axis at the horizon diminishes. At the same time, a pronounced minimum develops on the ρ -axis at the horizon, aggravating the angle-dependence of the energy density at the horizon.

With decreasing x_H the energy density of the matter fields of the black hole solutions tends increasingly towards the energy density of the globally regular solution, which possesses a toroidal shape because of the strong global maximum on the ρ -axis [8,4,9]. However, the limit $x_H \rightarrow 0$ is not smooth, as already observed in Sec. III for the static spherically symmetric solutions. The reason is, that the magnetic field of the black hole solutions is purely radial at the horizon, while the magnetic field of the globally regular solutions also has non-vanishing B_θ at the origin. In the static axially symmetric solutions, both B_r and B_θ are angle-dependent. For the globally regular solutions the contributions from both B_r and B_θ precisely add to an angle-independent density at the origin. In contrast, the black hole solutions possess an angle-dependent density at the horizon.

In Figs. 10–12 we show the functions of the black hole solutions with $n=2$, $k=1$, $\gamma=1$ and $x_H=0.01$, 0.1, 1 and 10 for three angles. Figure 10 shows the metric functions, Figs. 11 show the gauge field functions, and Fig. 12 shows the dilaton function. For small values of x_H , the angle-dependence of the metric functions is strongest around $x=1$. With increasing x_H , the angle-dependence decreases strongly, and the metric becomes increasingly spherical. At the same time, with increasing x_H the matter fields become less important. This is seen for instance in Fig. 13, where we

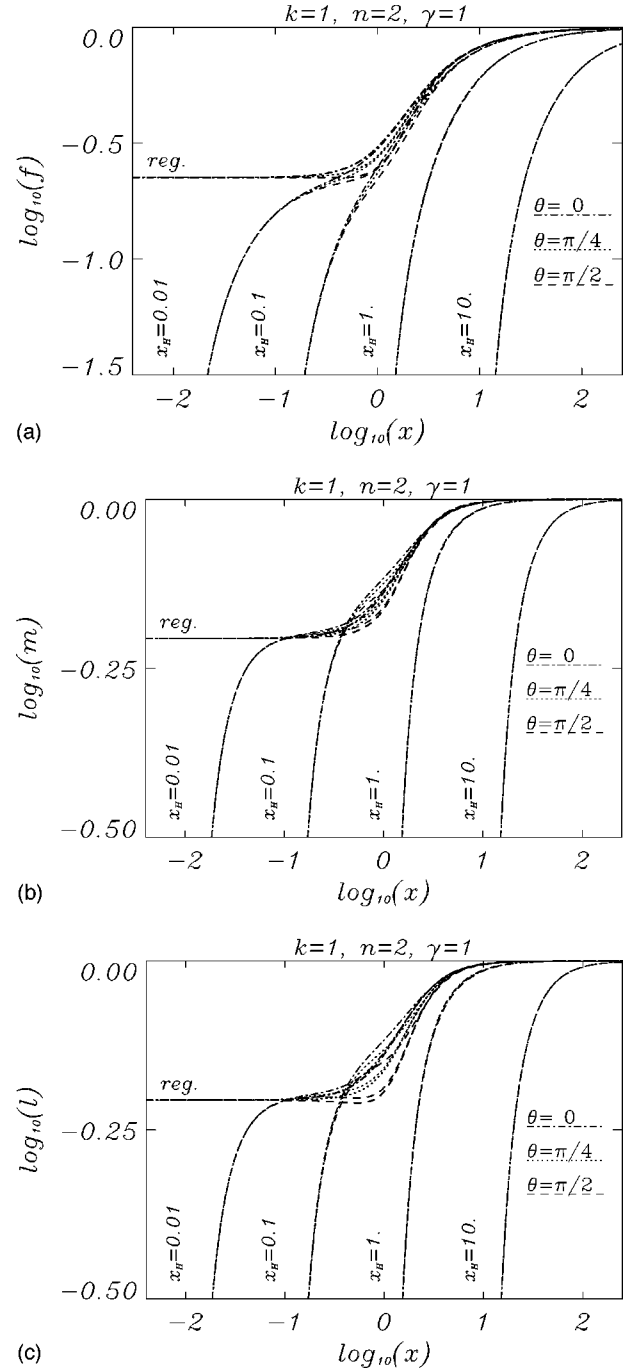


FIG. 10. (a) Same as Fig. 9 for the metric function f . (b) Same as Fig. 9 for the metric function m . (c) Same as Fig. 9 for the metric function l .

present relation (43), $\mu = \mu_o + 2TS$ (with $\mu_o = D/\gamma$), and observe that $\mu_o \gg 2TS$ for small x_H , whereas $\mu_o \ll 2TS$ for large x_H . Considering the gauge field functions, we recall that for the globally regular solutions the functions H_2 and H_4 have precisely k nodes, the function H_1 has $k-1$ non-trivial nodes, and the function H_3 has one non-trivial node [9]. For the black hole solutions we observe accordingly that H_1 has no node and that H_2 and H_4 each have one node. However, we observe two non-trivial nodes for the function H_3 of the black hole solutions of Fig. 11(c), which may be due to the choice of gauge. We note that the gauge field functions of Figs. 11 are obtained with gauge condition (19).

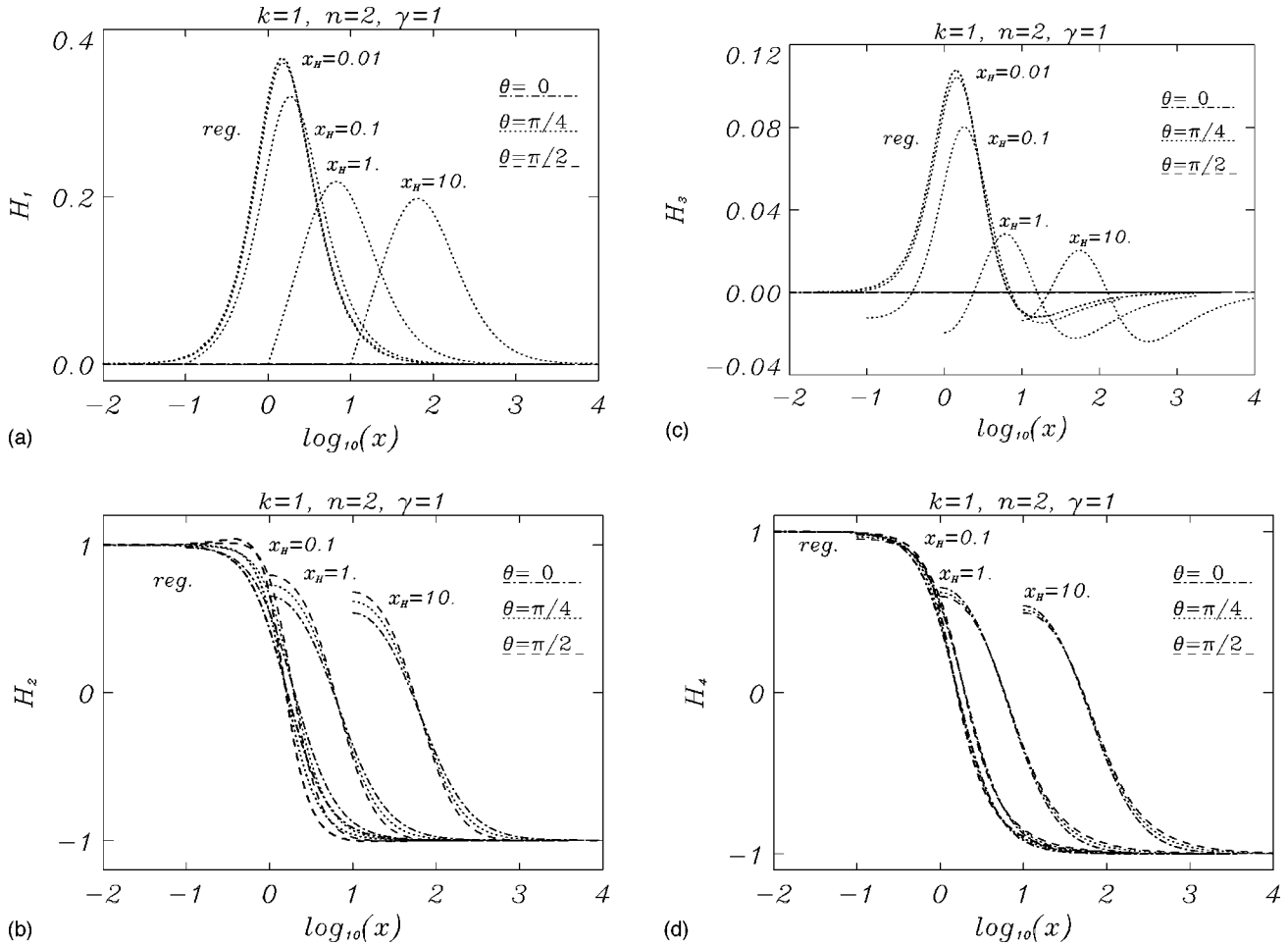


FIG. 11. (a) Same as Fig. 9 for the gauge field function H_1 . (b) Same as Fig. 9 for the gauge field function H_2 for horizon radii $x_H=0.1$, $x_H=1$, and $x_H=10$. (c) Same as Fig. 9 for the gauge field function H_3 . (d) Same as (b) for the gauge field function H_4 .

With increasing x_H the gauge field functions retain a considerable angle-dependence. They approach a limiting shape, shifting towards larger values of x . The dilaton function is slightly angle-dependent at the horizon, as seen in Fig. 12. Analogously to the metric functions, for small values of x_H the angle-dependence of the dilaton function is strongest around $x=1$. With increasing x_H the angle-dependence decreases strongly, and at the same time the magnitude of the

dilaton function diminishes strongly.

In Fig. 14 we exhibit the Kretschmann scalar for these solutions. With decreasing x_H the Kretschmann scalar of the black hole solutions tends to the Kretschmann scalar of the globally regular solution except close to the horizon, where it increases dramatically. For finite x_H , however, the

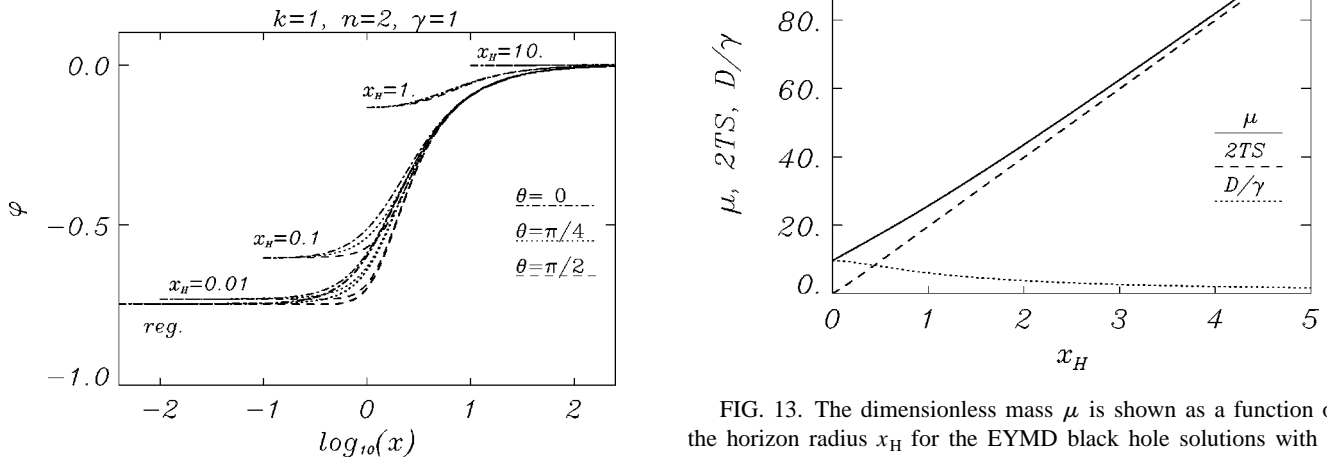


FIG. 12. Same as Fig. 9 for the dilaton function φ .

FIG. 13. The dimensionless mass μ is shown as a function of the horizon radius x_H for the EYMD black hole solutions with $\gamma=1$, winding number $n=2$, node number $k=1$. Also shown are $2TS$ and D/γ .

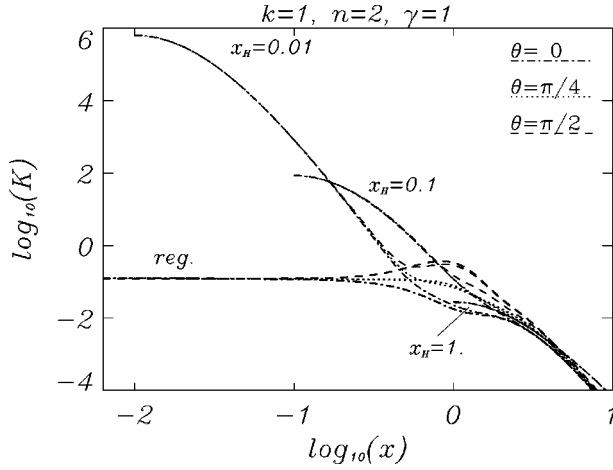


FIG. 14. The Kretschmann scalar is shown as a function of the dimensionless coordinate x for the angles $\theta=0$, $\theta=\pi/4$ and $\theta=\pi/2$ for the EYMD black hole solutions with $\gamma=1$, winding number $n=2$, node number $k=1$ and the horizon radii $x_H=1, 0.1$, and 0.01 , as well as for the corresponding globally regular solution.

Kretschmann scalar remains finite at the horizon, indicating that the black hole solutions indeed possess a regular horizon, as required (see Appendix A 2).

In general the EYM solutions are very similar to the EYMD solutions. We therefore do not exhibit these here. For instance, the energy density of the matter fields and the metric functions f and m for the EYM black hole solutions with $n=2$, $k=1$ and $x_H=0.02, 0.1, 0.5$ and 1 are shown in [4].

Let us now inspect the metric functions at the horizon more closely. In Figs. 15(a)–15(c) we exhibit the expansion coefficients $f_2(\theta)$, $m_2(\theta)$ and $l_2(\theta)$ of the metric functions for the above set of EYMD solutions. With increasing x_H the angle-dependence of the expansion coefficients first increases and then decreases again. The shape of the horizon changes with x_H in a similar way. This is seen in Fig. 16, where the ratio of the circumference at the equator and the circumference at the poles, L_e/L_p , is shown as a function of the mass for the EYMD ($\gamma=1$) and EYM black hole solutions with $n=2$ and $k=1$. The maximal deformation of the horizon occurs for an isotropic horizon radius of $x_H=0.295$ for $\gamma=1$ and $x_H=0.195$ for $\gamma=0$. For $\gamma=0$, the maximal deformation of the horizon is greater than for $\gamma=1$. Figure 17 shows the area of the horizon as a function of the mass for the corresponding solutions. For comparison, the area of a spherical horizon with circumference L_e is also shown, deviating only little from the area of the deformed horizon.

Figure 18 shows the inverse temperature as a function of the mass for the static axially symmetric EYMD ($\gamma=1$) and EYM black hole solutions with $n=2$ and $k=1$. These curves are very similar to those of the corresponding static spherically symmetric black hole solutions [23]. Table I presents the dimensionless mass, temperature, entropy and dilaton charge as well as the ratio L_e/L_p of the above set of static axially symmetric black hole solutions of EYMD theory ($\gamma=1$).

C. Winding number dependence

To illustrate the winding number dependence of the black hole solutions we show in Figs. 19 the solutions with n

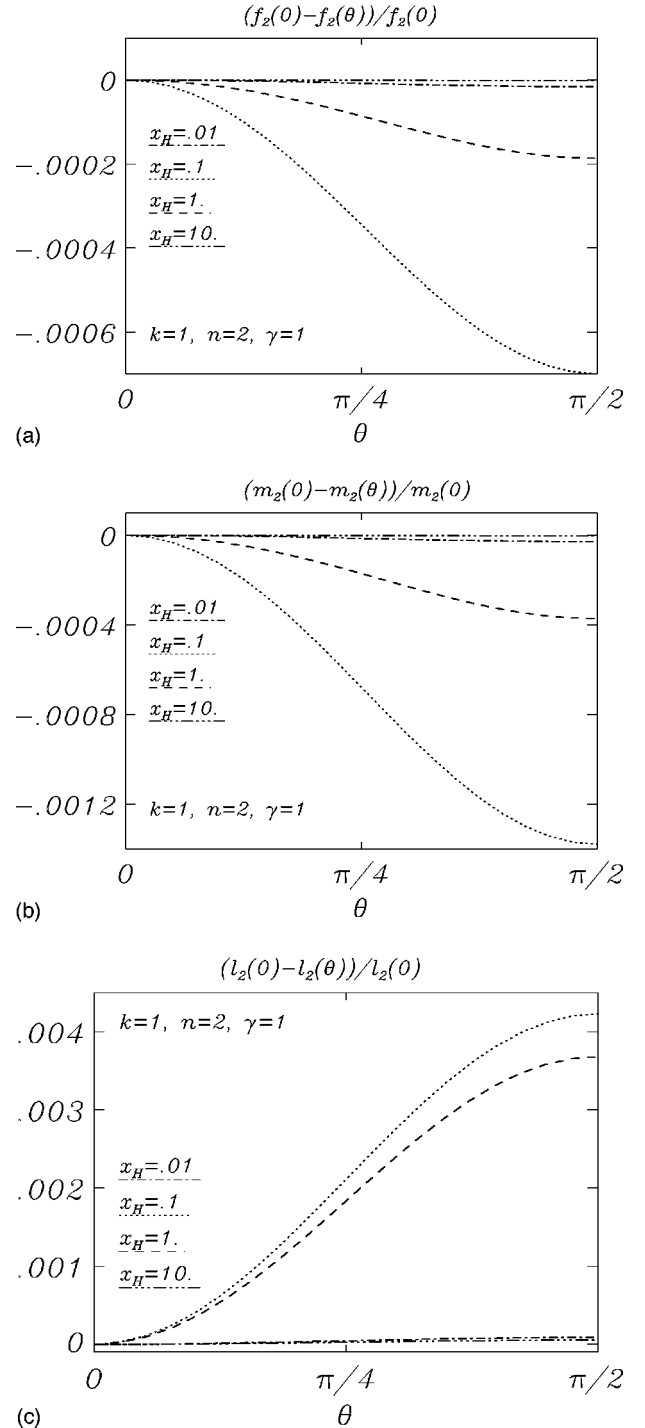


FIG. 15. (a) The normalized expansion coefficient f_2 of the metric function f is shown as a function of the angle θ for the EYMD black hole solutions with $\gamma=1$, winding number $n=2$, node number $k=1$ and the horizon radii $x_H=10, 1, 0.1$, and 0.01 . (b) Same as (a) for the expansion coefficient m_2 of the metric function m . (c) Same as (a) for the expansion coefficient l_2 of the metric function l .

$=4$, $k=1$, $\gamma=1$ and $x_H=0.01, 0.1, 1$ and 10 for three angles. In Fig. 19(a) we see the energy density of the matter fields. We recall, that with increasing winding number n the maximum on the ρ -axis of the energy density of the globally regular solutions shifts outward and decreases in height [9]. As compared to the $n=2$ black hole solutions, shown in Fig.

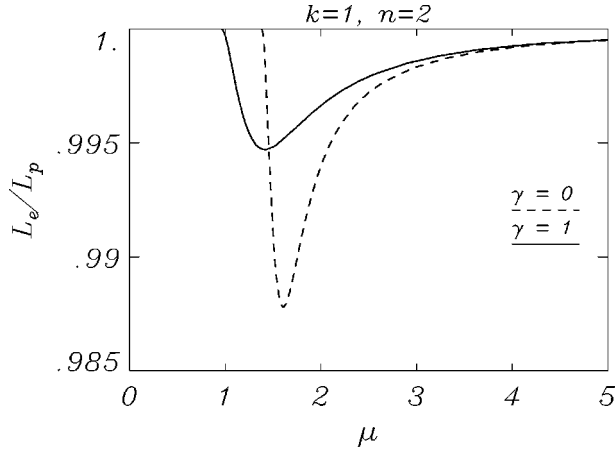


FIG. 16. The ratio L_e/L_p of the circumference of the horizon along the equator L_e to the circumference of the horizon along the poles L_p is shown as a function of the dimensionless mass μ for the black hole solutions with winding number $n=2$ and node number $k=1$ of EYMD theory with $\gamma=1$ and EYM theory.

9, we here observe that with decreasing x_H the globally regular solution is approached faster for the greater winding number $n=4$, while with increasing x_H the angle-dependence of the energy density of the black hole solutions remains stronger. Most strikingly, however, we observe, that the global maximum always resides on the ρ -axis. The maximum on the z -axis remains a local one also for large x_H .

In Figs. 19(b)–19(d) we show the metric function f , the gauge field function H_2 and the dilaton function φ , respectively. For the globally regular solutions the angle-dependence of the metric and matter functions increases strongly with n and the location of the biggest angular splitting moves further outward. This dependence is reflected in the black hole solutions. In particular we observe, that with increasing n the angular dependence remains stronger for larger x_H .

Let us now turn to the shape of the horizon. As for $n=2$, with increasing x_H the ratio of the circumference at the equator and the circumference at the poles, L_e/L_p , first decreases and then increases again. In Fig. 20 the ratio L_e/L_p is shown as a function of the mass for the EYMD ($\gamma=1$) and EYM black hole solutions with $n=4$ and $k=1$. The maximal

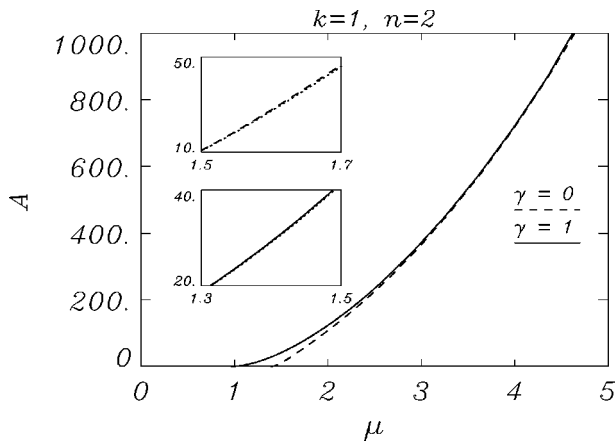


FIG. 17. Same as Fig. 16 for the area A of the horizon.

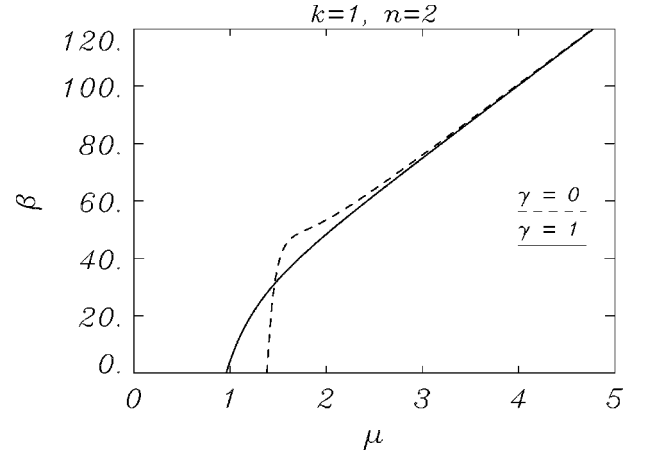


FIG. 18. Same as Fig. 16 for the inverse temperature $\beta = T^{-1}$.

deformation of the horizon occurs for an isotropic horizon radius of $x_H=0.95$ for $\gamma=1$ and $x_H=0.65$ for $\gamma=0$. Again, for $\gamma=0$ the maximal deformation of the horizon is greater than for $\gamma=1$, but for $n=4$ it is smaller than for $n=2$. Table I presents the ratio L_e/L_p as well as the dimensionless mass,

TABLE I. The dimensionless mass μ , the temperature T , the entropy S , the dilaton charge D and the ratio L_e/L_p of the EYMD black hole solutions with node number $k=1$ and winding number $n=2$, $k=1$ and $n=4$, as well as $k=2$ and $n=2$ are shown for the values of the horizon radius $x_H=0.01$, 0.1 , 1 and 10 .

x_H	EYMD($\gamma=1$)		
	$k=1, n=2$	$k=1, n=4$	$k=2, n=2$
μ			
0.01	0.9766	1.6227	1.2762
0.1	1.1183	1.7700	1.4081
1.	2.5649	3.2193	2.5649
10	20.079	20.244	20.079
T			
0.01	0.583	0.989	0.230
0.1	0.727	0.076	0.039
1.	0.016	0.013	0.016
10.	0.002	0.002	0.002
S			
0.01	0.014	0.012	0.033
0.1	1.167	1.116	2.243
1.	62.47	71.25	62.47
10.	5045.	5081.	5045.
D			
0.01	0.9609	1.6063	1.2619
0.1	0.9487	1.6011	1.2319
1.	0.6022	1.3188	0.6023
10.	0.0836	0.2682	0.0836
L_e/L_p			
0.01	0.9999	1.0000	0.9993
0.1	0.9974	0.9997	0.9910
1.	0.9980	0.9968	0.9980
10.	1.0000	0.9998	1.0000

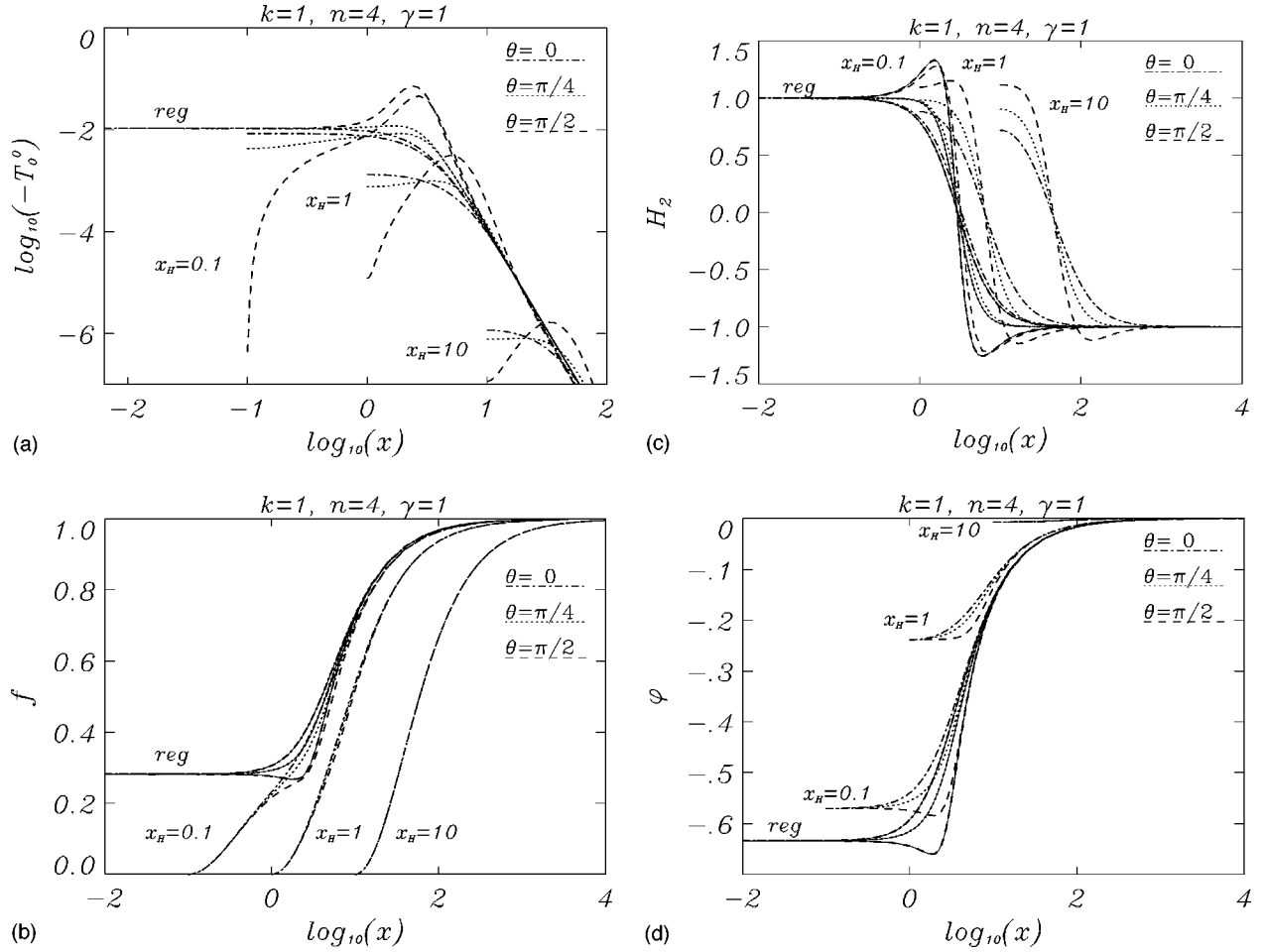


FIG. 19. (a) The energy density $\epsilon = -T_0^0$ is shown as a function of the dimensionless coordinate x for the angles $\theta=0$, $\theta=\pi/4$ and $\theta=\pi/2$ for the EYMD black hole solutions with $\gamma=1$, winding number $n=4$, node number $k=1$ and horizon radii $x_H=0.1$, $x_H=1$, and $x_H=10$, as well as for the corresponding globally regular solution. (b) Same as (a) for the metric function f . (c) Same as (a) for the gauge field function H_2 . (d) Same as (a) for the dilaton function φ .

temperature, entropy and dilaton charge for the above set of static axially symmetric black hole solutions of EYMD theory ($\gamma=1$).

D. Node number dependence

To illustrate the node number dependence of the black hole solutions we show in Figs. 21 the solutions with $n=2$, $k=2$, $\gamma=1$ and the same set of radii x_H as above. The energy density of the matter fields is shown in Fig. 21(a). We recall that the maximum of the energy density of the globally regular solutions is located on the ρ -axis. With increasing node number k it shifts inward and increases strongly in height [9]. For the black hole solutions we observe that with decreasing x_H the globally regular solution is approached more slowly for greater node number k , while with increasing x_H the angle-dependence of the energy density of the black hole solutions diminishes faster. In particular, for large x_H the maximum on the z -axis becomes the global maximum, while the maximum on the ρ -axis disappears.

In Figs. 21(b)–21(d) we show the metric function f , the gauge field function H_2 and the dilaton function φ , respectively. We recall, that for the globally regular solutions the location of the biggest angular splitting moves inward with k while its size stays roughly constant for most functions [9].

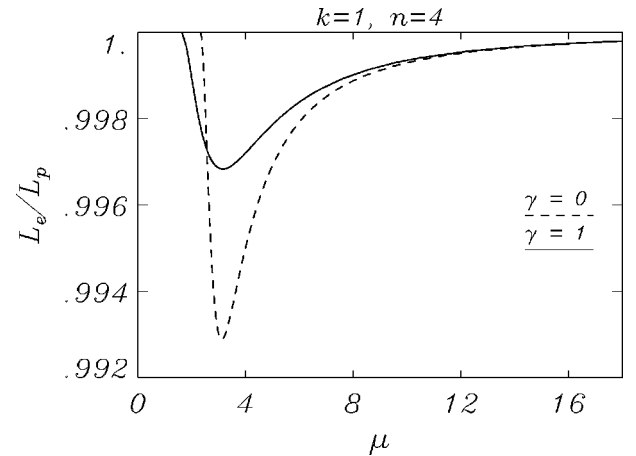


FIG. 20. The ratio L_e/L_p of the circumference of the horizon along the equator L_e to the circumference of the horizon along the poles L_p is shown as a function of the dimensionless mass μ for the black hole solutions with winding number $n=4$ and node number $k=1$ of EYMD theory with $\gamma=1$ and EYM theory.

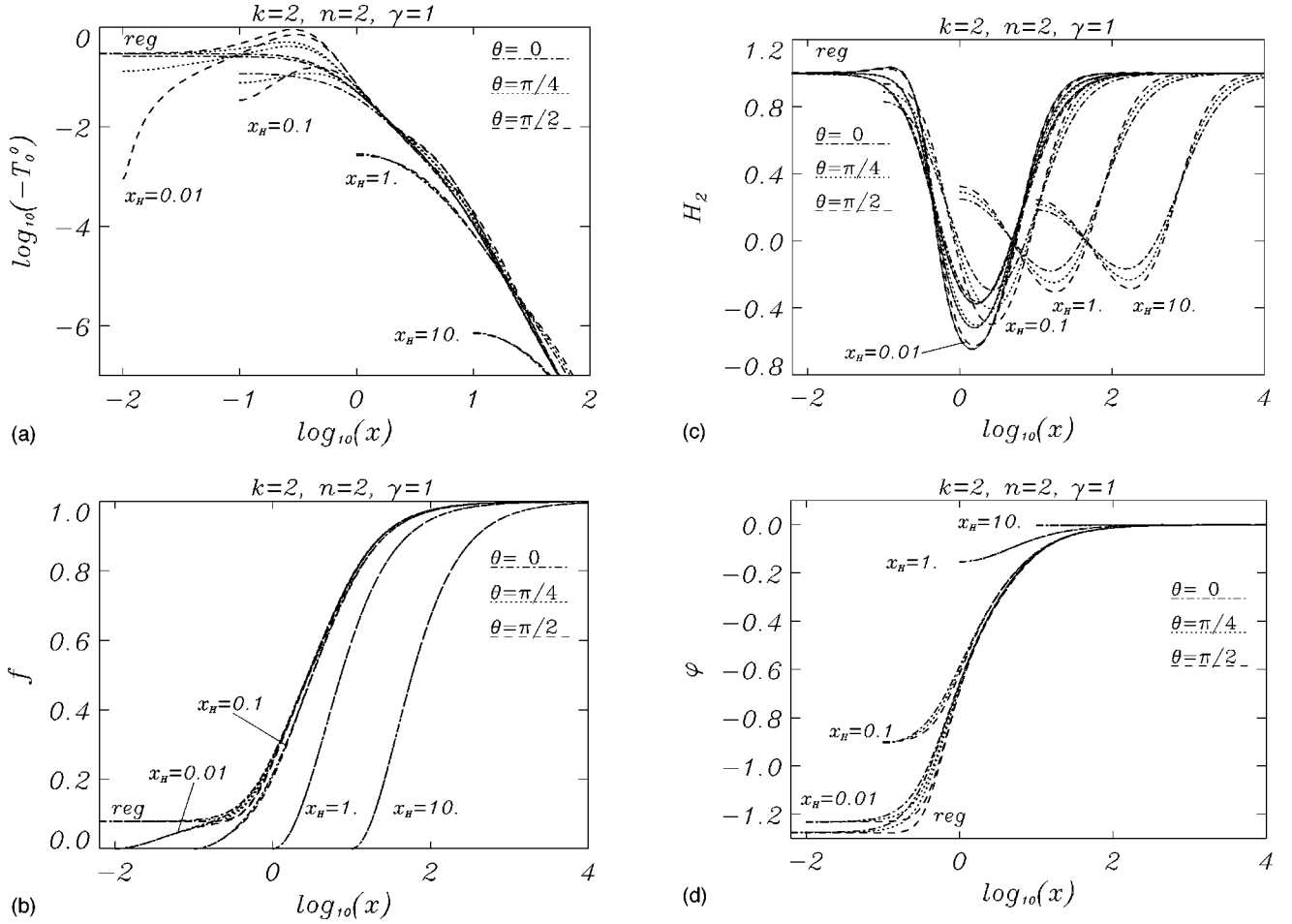


FIG. 21. (a) The energy density $\epsilon = -T_0^0$ is shown as a function of the dimensionless coordinate x for the angles $\theta=0$, $\theta=\pi/4$ and $\theta=\pi/2$ for the EYMD black hole solutions with $\gamma=1$, winding number $n=2$, node number $k=2$ and horizon radii $x_H=0.01$, $x_H=0.1$, $x_H=1$, and $x_H=10$, as well as for the corresponding globally regular solution. (b) Same as (a) for the metric function f . (c) Same as (a) for the gauge field function H_2 . (d) Same as (a) for the dilaton function φ .

For the black hole solutions we here observe, that as compared to the $k=1$ solutions, shown in Figs. 10–12, the angular dependence of the metric and dilaton functions diminishes faster with increasing x_H .

Table I again shows the dimensionless mass, temperature, entropy and dilaton charge as well as the ratio L_e/L_p for the above set of static axially symmetric black hole solutions of EYMD theory ($\gamma=1$).

E. Limiting solutions

For fixed n , γ and x_H and increasing k , the static axially symmetric black hole solutions form sequences, tending to limiting solutions. Whereas the solutions of the sequences are magnetically neutral, axially symmetric and non-Abelian, the limiting solutions possess magnetic charge n and they are spherically symmetric and Abelian. For finite γ the limiting solutions are EMD black hole solutions [13], while for $\gamma=0$ the limiting solutions are Reissner-Nordström solutions [4,9]. The convergence of the global properties is seen for instance in Table I of [4].

To illustrate the convergence of the metric and matter functions, we exhibit in Figs. 22(a)–22(c) the EYMD solu-

tions for $n=2$, $\gamma=1$ and $x_H=1$ as an example. With increasing k , the metric functions converge rapidly to the metric functions of the limiting EMD solution. In Fig. 22(a) this is seen for the metric function f . With increasing k , the gauge field functions tend to their (vanishing) limiting functions in an exponentially increasing interval, but because of the boundary conditions the convergence is not uniform for H_2 and H_4 . This is illustrated in Fig. 22(b) for the gauge field function H_2 . The dilaton function shown in Fig. 22(c) again converges rapidly and uniformly.

V. CONCLUSIONS

We have constructed numerically a new class of black hole solutions in EYM and EYMD theory [4]. These black hole solutions are asymptotically flat, static and possess a regular event horizon. However, they are not spherically symmetric but only axially symmetric with angle-dependent fields at the horizon.

The event horizon of the static axially symmetric black

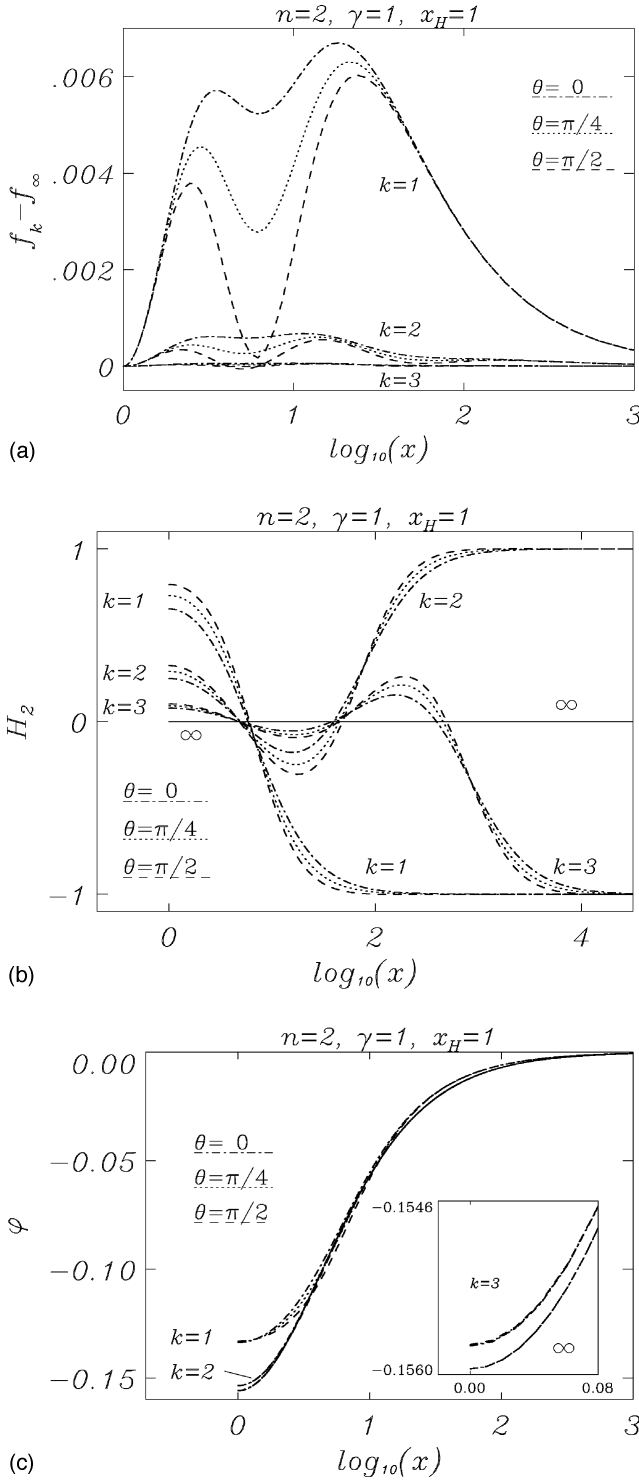


FIG. 22. (a) The difference of the metric function f_k and the metric function f_∞ of the limiting solution is shown as a function of the dimensionless coordinate x for the angles $\theta=0$, $\theta=\pi/4$ and $\theta=\pi/2$ for the EYMD black hole solutions with $\gamma=1$, horizon radius $x_H=1$, winding number $n=2$, and node numbers $k=1-3$. (b) The gauge field function H_2 is shown as a function of the dimensionless coordinate x for the angles $\theta=0$, $\theta=\pi/4$ and $\theta=\pi/2$ for the EYMD black hole solutions with $\gamma=1$, horizon radius $x_H=1$, winding number $n=2$, and node numbers $k=1-3$. Also shown is the gauge field function of the limiting EMD solution. (c) Same as (b) for the dilaton function φ .

hole solutions resides at a surface of constant isotropic radial coordinate, $x=x_H$. However, the horizon is not spherical. Evaluating the circumference of the horizon along the equator L_e and the circumference of the horizon along the poles L_p , we observe that the ratio L_e/L_p is slightly smaller than one, i.e., the horizon is slightly elongated along the symmetry axis, the maximal elongation occurring for small values of x_H .

Like their globally regular counterparts, the static axially symmetric black hole solutions are characterized by two integers, the winding number $n>1$ and the node number k of the purely magnetic gauge field. Whereas the energy density of the globally regular solutions has a toruslike shape, due to a strong peak on the ρ -axis away from the origin [8], the energy density of the black hole solutions has a more complicated shape, depending on the winding number n , the node number k and the horizon radius x_H .

The static spherically symmetric EYM and EYMD black hole solutions are unstable [27,12], and there is all reason to believe, that the static axially symmetric black hole solutions are unstable, too. But we expect analogous black hole solutions in EYMH theory [5,28] and ES theory [29], corresponding to black holes inside axially symmetric multimonopoles and multiskyrmions, respectively, and for $n=2$ these static axially symmetric solutions should be stable [5,28,29]. In contrast, stable black hole solutions with higher magnetic charges (EYMH) or higher baryon numbers (ES) should not correspond to static axially symmetric solutions with $n>2$. Instead these stable black hole solutions should exhibit only discrete crystal-like symmetries [5,28,29]. We expect analogous but unstable black hole solutions with crystal-like symmetries also in EYM and EYMD theory.

ACKNOWLEDGMENT

We would like to thank the RRZN in Hannover for computing time.

APPENDIX A

1. Expansion at the horizon

Here we present the expansion of the functions of the static axially symmetric black hole solutions at the horizon x_H in powers of δ ,

$$\delta = \frac{x}{x_H} - 1. \quad (\text{A1})$$

The expansion of the functions at the horizon can be obtained from the regularity conditions imposed on the Einstein equations and the matter field equations:

$$\begin{aligned}
f(\delta, \theta) &= \delta^2 f_2 \left\{ 1 - \delta + \frac{\delta^2}{24} \left[\frac{f_2}{l_2} \left(\frac{n}{x_H} \right)^2 e^{2\gamma\varphi_0} \left[24 \cot \theta [(H_{30,\theta} + 1 - H_{20}^2) H_{30} - H_{20} H_{40,\theta} + H_{40} H_{40,\theta}] + 12 \left(H_{20}^2 (H_{30}^2 + H_{40}^2 - 1) \right. \right. \right. \right. \\
&\quad \left. \left. \left. + \frac{(H_{20} - H_{40})^2 + H_{30}^2}{\sin^2 \theta} - (H_{30}^2 + H_{40}^2) + 2 H_{20} (H_{30} H_{40,\theta} - H_{40} H_{30,\theta}) + 1 + 2 H_{30,\theta} + H_{30,\theta}^2 + H_{40,\theta}^2 \right) \right] \right. \\
&\quad \left. \left. - 2 \cot \theta \left(3 \frac{f_{2,\theta}}{f_2} - 2 \frac{l_{2,\theta}}{l_2} \right) - \left(3 \frac{f_{2,\theta}}{f_2} \frac{l_{2,\theta}}{l_2} + 6 \frac{f_{2,\theta\theta}}{f_2} + \left(\frac{l_{2,\theta}}{l_2} \right)^2 - 2 \frac{l_{2,\theta\theta}}{l_2} - 18 - 6 \left(\frac{f_{2,\theta}}{f_2} \right)^2 \right) \right] \right\} + O(\delta^5), \\
m(\delta, \theta) &= \delta^2 m_2 \left\{ 1 - 3\delta + \frac{\delta^2}{24} \left[150 - 4 \frac{l_{2,\theta,\theta}}{l_2} + 2 \left(\frac{l_{2,\theta}}{l_2} \right)^2 + 3 \frac{l_{2,\theta}}{l_2} \frac{m_{2,\theta}}{m_2} - 6 \frac{m_{2,\theta,\theta}}{m_2} + 6 \left(\frac{m_{2,\theta}}{m_2} \right)^2 - 6 \left(\frac{f_{2,\theta}}{f_2} \right)^2 \right. \right. \\
&\quad \left. \left. + 2 \cot \theta \left(3 \frac{m_{2,\theta}}{m_2} - 4 \frac{l_{2,\theta}}{l_2} \right) - 24 \varphi_{0,\theta}^2 \right] \right\} + O(\delta^5), \\
l(\delta, \theta) &= \delta^2 l_2 \left\{ 1 - 3\delta + \frac{\delta^2}{12} \left[\left(\frac{l_{2,\theta}}{l_2} \right)^2 - 2 \frac{l_{2,\theta\theta}}{l_2} + 75 - 4 \cot \theta \frac{l_{2,\theta}}{l_2} \right] \right\} + O(\delta^5), \\
H_1(\delta, \theta) &= \delta \left(1 - \frac{\delta}{2} \right) H_{11} + O(\delta^3), \\
H_2(\delta, \theta) &= H_{20} + \frac{\delta^2}{4} \left[\frac{m_2}{l_2} n^2 \left(H_{20} (H_{30}^2 + H_{40}^2 - 1) + H_{30} H_{40,\theta} - H_{40} H_{30,\theta} + \frac{H_{20} - H_{40}}{\sin^2 \theta} \right. \right. \\
&\quad \left. \left. - \cot \theta (2 H_{20} H_{30} + H_{40,\theta}) \right) + (H_{11,\theta} - H_{20,\theta\theta}) \right] + O(\delta^3), \\
H_3(\delta, \theta) &= H_{30} - \frac{\delta^2}{8} \left[\left(4 \gamma \varphi_{0,\theta} + 2 \frac{f_{2,\theta}}{f_2} - \frac{l_{2,\theta}}{l_2} \right) (1 - H_{40} H_{20} + H_{30,\theta} + \cot \theta H_{30}) + 2 \cot \theta H_{20} (H_{20} - H_{40}) + 2 H_{30,\theta\theta} - 4 H_{20} H_{40,\theta} \right. \\
&\quad \left. - 2 \left(\frac{H_{30}}{\sin^2 \theta} - \cot \theta H_{30,\theta} \right) - 2 H_{30} H_{20}^2 - 2 H_{40} (2 H_{11} + H_{20,\theta}) \right] + O(\delta^3), \\
H_4(\delta, \theta) &= H_{40} - \frac{\delta^2}{8} \left[\left(4 \gamma \varphi_{0,\theta} + 2 \frac{f_{2,\theta}}{f_2} - \frac{l_{2,\theta}}{l_2} \right) [H_{40,\theta} + H_{30} H_{20} - \cot \theta (H_{20} - H_{40})] + H_{20} (4 H_{30,\theta} + 2) + 2 [H_{30} (2 H_{11} + H_{20,\theta}) \right. \\
&\quad \left. + H_{40,\theta\theta} - H_{40} H_{20}^2] + 2 \frac{H_{20} - H_{40}}{\sin^2 \theta} - 2 \cot \theta (2 H_{11} - H_{40,\theta} - H_{20} H_{30} + H_{20,\theta}) \right] + O(\delta^3), \\
\varphi(\delta, \theta) &= \varphi_0 - \frac{\delta^2}{8} \left\{ 2 \varphi_{0,\theta} \cot \theta + \varphi_{0,\theta} \frac{l_{2,\theta}}{l_2} + 2 \varphi_{0,\theta\theta} - \frac{f_2}{l_2} \frac{n^2}{x_H^2} \gamma e^{2\gamma\varphi_0} \left[4 \cot \theta [H_{30} (H_{30,\theta} + 1) - H_{20} (H_{20} H_{30} + H_{40,\theta}) + H_{40} H_{40,\theta}] \right. \right. \\
&\quad \left. \left. + 2 \left((H_{30}^2 + H_{40}^2 - 1) H_{20}^2 + 2 H_{20} (H_{30} H_{40,\theta} - H_{40} H_{30,\theta}) + H_{30,\theta}^2 + 2 H_{30,\theta} + H_{40,\theta}^2 + 1 + \frac{(H_{20} - H_{40})^2}{\sin^2 \theta} + \frac{H_{30}^2}{\sin^2 \theta} \right. \right. \right. \\
&\quad \left. \left. \left. - (H_{30}^2 + H_{40}^2) \right) \right] \right\} + O(\delta^3) \tag{A2}
\end{aligned}$$

The expansion coefficients f_2 , m_2 , l_2 , H_{11} , H_{20} , H_{30} , H_{40} and φ_0 are functions of the variable θ . The expansion depends on the gauge condition imposed on the gauge field functions at the horizon. For the expansion above we employed the gauge condition (19), $(\partial_\theta H_1)|_{x=x_H} = 0$.

The expansion of the functions at infinity is given in [9].

2. Kretschmann scalar

Here we derive the expression for the Kretschmann scalar K , Eq. (70), for the static axially symmetric black hole solutions and show that it is finite at the horizon.

The nonvanishing components of the Riemann tensor are

$$\begin{aligned}
 R_{0r0r} &= \frac{f}{4r^2} \left[\frac{f_{,\theta}}{f} \left(\frac{m_{,\theta}}{m} - \frac{f_{,\theta}}{f} \right) - r^2 \left(\frac{f_{,r}}{f} \frac{m_{,r}}{m} - 2 \frac{f_{,r,r}}{f} \right) \right] = -R_{0rr0} = -R_{r00r} = R_{r0r0}, \\
 R_{0r0\theta} &= -\frac{f}{4r} \left[\left(2 + r \frac{m_{,r}}{m} - r \frac{f_{,r}}{f} \right) \frac{f_{,\theta}}{f} + r \frac{f_{,r}}{f} \frac{m_{,\theta}}{m} - 2r \frac{f_{,r,\theta}}{f} \right] = -R_{0r\theta 0} = -R_{r00\theta} = R_{r0\theta 0} = R_{0\theta 0r} = -R_{0\theta r0} = -R_{\theta 00r} = R_{\theta 0r0}, \\
 R_{0\theta 0\theta} &= \frac{f}{4} \left[r \frac{f_{,r}}{f} \left(2 - r \frac{f_{,r}}{f} + r \frac{m_{,r}}{m} \right) - \frac{f_{,\theta}}{f} \frac{m_{,\theta}}{m} + 2 \frac{f_{,\theta,\theta}}{f} \right] = -R_{0\theta\theta 0} = -R_{\theta 00\theta} = R_{\theta 0\theta 0}, \\
 R_{0\phi 0\phi} &= -\frac{fl}{4m} \sin^2 \theta \left[r \frac{f_{,r}}{f} \left(r \frac{f_{,r}}{f} - r \frac{l_{,r}}{l} - 2 \right) + \frac{f_{,\theta}}{f} \left(\frac{f_{,\theta}}{f} - \frac{l_{,\theta}}{l} - 2 \cot \theta \right) \right] = -R_{0\phi\phi 0} = -R_{\phi 00\phi} = R_{\phi 0\phi 0}, \\
 R_{r\theta r\theta} &= -\frac{m}{2f} \left[r \frac{m_{,r}}{m} - r \frac{f_{,r}}{f} + r^2 \left(\frac{m_{,r,r}}{m} - \frac{f_{,r,r}}{f} \right) + \frac{m_{,\theta,\theta}}{m} - \frac{f_{,\theta,\theta}}{f} - \left[\left(r \frac{m_{,r}}{m} \right)^2 - \left(r \frac{f_{,r}}{f} \right)^2 \right] - \left[\left(\frac{m_{,\theta}}{m} \right)^2 - \left(\frac{f_{,\theta}}{f} \right)^2 \right] \right] \\
 &= -R_{r\theta\theta r} = -R_{\theta rr\theta} = R_{\theta r\theta r}, \\
 R_{r\phi r\phi} &= -\frac{l}{4f} \sin^2 \theta \left[\left(\frac{l_{,\theta}}{l} - \frac{f_{,\theta}}{f} + 2 \cot \theta \right) \left(\frac{m_{,\theta}}{m} - \frac{f_{,\theta}}{f} \right) - \left(r \frac{l_{,r}}{l} - r \frac{f_{,r}}{f} + 2 \right) \left(r \frac{m_{,r}}{m} + 3r \frac{f_{,r}}{f} \right) + 2 \left(r^2 \frac{l_{,r,r}}{l} + 4r \frac{l_{,r}}{l} - r^2 \frac{f_{,r,r}}{f} + 2 \right) \right. \\
 &\quad \left. - \left(r \frac{l_{,r}}{l} - r \frac{f_{,r}}{f} + 2 \right)^2 \right] \\
 &= -R_{r\phi\phi r} = -R_{\phi rr\phi} = R_{\phi r\phi r}, \\
 R_{\theta\phi\theta\phi} &= -\frac{l}{4f} r^2 \sin^2 \theta \left[2 \cot \theta \left(2 \frac{l_{,\theta}}{l} - \frac{m_{,\theta}}{m} - \frac{f_{,\theta}}{f} \right) + 2r \frac{l_{,r}}{l} + 2r \frac{m_{,r}}{m} - 4r \frac{f_{,r}}{f} + r \frac{m_{,r}}{m} r \frac{l_{,r}}{l} - r \frac{f_{,r}}{f} r \frac{l_{,r}}{l} - r \frac{m_{,r}}{m} r \frac{f_{,r}}{f} + \left(r \frac{f_{,r}}{f} \right)^2 \right. \\
 &\quad \left. + 2 \frac{l_{,\theta,\theta}}{l} - \left(\frac{l_{,\theta}}{l} \right)^2 - 2 \frac{f_{,\theta,\theta}}{f} + 2 \left(\frac{f_{,\theta}}{f} \right)^2 - \frac{m_{,\theta}}{m} \frac{l_{,\theta}}{l} - \frac{f_{,\theta}}{f} \frac{l_{,\theta}}{l} + \frac{m_{,\theta}}{m} \frac{f_{,\theta}}{f} \right] \\
 &= -R_{\theta\phi\phi\theta} = -R_{\phi\theta\theta\phi} = R_{\phi\theta\phi\theta}, \\
 R_{r\phi\theta\phi} &= -\frac{l}{4f} r \sin^2 \theta \left[2 \cot \theta \left(r \frac{l_{,r}}{l} - r \frac{m_{,r}}{m} \right) + 2 \left(r \frac{l_{,r,\theta}}{l} - r \frac{f_{,r,\theta}}{f} \right) - r \frac{l_{,r}}{l} \frac{l_{,\theta}}{l} - \left[r \frac{m_{,r}}{m} \left(\frac{l_{,\theta}}{l} - \frac{f_{,\theta}}{f} \right) + \frac{m_{,\theta}}{m} \left(r \frac{l_{,r}}{l} - r \frac{f_{,r}}{f} \right) \right] \right. \\
 &\quad \left. - 2 \left(\frac{m_{,\theta}}{m} - \frac{f_{,\theta}}{f} \right) + r \frac{f_{,r}}{f} \frac{f_{,\theta}}{f} \right] \\
 &= -R_{r\phi\phi\theta} = -R_{\phi r\theta\phi} = R_{\phi r\phi\theta} = R_{\theta\phi r\phi} = -R_{\theta\phi\phi r} = -R_{\phi\theta r\phi} = R_{\phi\theta\phi r}.
 \end{aligned}$$

The Kretschmann scalar $K = R_{\mu\nu\lambda\rho} R^{\mu\nu\lambda\rho}$ is then given by

$$\begin{aligned}
 K &= 4[(R_{0r0r} g^{00} g^{rr})^2 + (R_{0\theta 0\theta} g^{00} g^{\theta\theta})^2 + (R_{0\phi 0\phi} g^{00} g^{\phi\phi})^2 \\
 &\quad + (R_{r\theta r\theta} g^{rr} g^{\theta\theta})^2 + (R_{r\phi r\phi} g^{rr} g^{\phi\phi})^2 + (R_{\theta\phi\theta\phi} g^{\theta\theta} g^{\phi\phi})^2] \\
 &\quad + 8[(R_{0r0\theta} g^{00})^2 + (R_{r\phi\theta\phi} g^{\phi\phi})^2] g^{rr} g^{\theta\theta}.
 \end{aligned}$$

becomes

$$\left(r \frac{f_{,r}}{f} \frac{m_{,\theta}}{m} - 2r \frac{f_{,r,\theta}}{f} \right) \frac{2r}{r - r_H} \left(\frac{m_{2,\theta}}{m_2} - 2 \frac{f_{2,\theta}}{f_2} \right),$$

which does not diverge because of relation (37). In terms like

In order to show that the Kretschmann scalar is finite at the horizon, we insert the expansion of the metric functions Eqs. (33) and (34) into the Riemann tensor. The term

$$\left(\frac{f_{,r}}{f} - \frac{m_{,r}}{m} \right)$$

and

$$\left(\frac{f_{,r,r}}{f} - \frac{m_{,r,r}}{m} \right)$$

the divergences cancel. Thus the Kretschmann scalar is indeed finite at the horizon.

APPENDIX B

Here we discuss our final choice of functions for the numerical integration.

At the horizon the expansion coefficients $f_2(\theta)$, $m_2(\theta)$ and $l_2(\theta)$ are of particular interest, because they enter into the expressions for the temperature, the area and the circumferences. In order to obtain these functions directly we have introduced the new functions $\bar{f}(\bar{x}, \theta)$, $\bar{m}(\bar{x}, \theta)$ and $\bar{l}(\bar{x}, \theta)$,

$$\begin{aligned} f(\bar{x}, \theta) &= \bar{x}^2 \bar{f}(\bar{x}, \theta), & m(\bar{x}, \theta) &= \bar{x}^2 \bar{m}(\bar{x}, \theta), \\ l(\bar{x}, \theta) &= \bar{x}^2 \bar{l}(\bar{x}, \theta), \end{aligned} \quad (\text{B1})$$

where $\bar{x} = (1 - x_H/x)$ is the compactified coordinate, Eq. (71). The functions $f_2(\theta)$, $m_2(\theta)$ and $l_2(\theta)$ are then given by

$$\begin{aligned} f_2(\theta) &= \frac{1}{x_H^2} \bar{f}(0, \theta), & m_2(\theta) &= \frac{1}{x_H^2} \bar{m}(0, \theta), \\ l_2(\theta) &= \frac{1}{x_H^2} \bar{l}(0, \theta). \end{aligned} \quad (\text{B2})$$

In the limit $x \rightarrow \infty$ the variable \bar{x} approaches the value 1. Consequently, at infinity the boundary conditions for the new functions \bar{f} , \bar{m} and \bar{l} coincide with the boundary conditions of the functions f , m and l , respectively. At the horizon the boundary conditions for the new functions can be obtained from the expansion of the metric functions. They are given by

$$(\bar{f} - \partial_{\bar{x}} \bar{f})|_{\bar{x}=0} = 0, \quad (\bar{m} + \partial_{\bar{x}} \bar{m})|_{\bar{x}=0} = 0, \quad (\bar{l} + \partial_{\bar{x}} \bar{l})|_{\bar{x}=0} = 0. \quad (\text{B3})$$

To satisfy the regularity condition (6) exactly in the numerical calculations, we have introduced the function $g(\bar{x}, \theta)$,

$$g(\bar{x}, \theta) = \frac{\bar{m}(\bar{x}, \theta)}{\bar{l}(\bar{x}, \theta)}. \quad (\text{B4})$$

On the symmetry axis this function satisfies the boundary condition

$$g|_{\theta=0} = 1 \quad (\text{B5})$$

and at the horizon

$$\partial_{\bar{x}} g|_{\bar{x}=0} = 0. \quad (\text{B6})$$

The numerical calculations were mostly performed with the functions $\bar{f}(\bar{x}, \theta)$, $g(\bar{x}, \theta)$ and $\bar{l}(\bar{x}, \theta)$.

-
- [1] See, e.g., A. E. Mayo and J. D. Bekenstein, *Phys. Rev. D* **54**, 5059 (1996).
 - [2] W. Israel, *Commun. Math. Phys.* **8**, 245 (1968); D. C. Robinson, *Phys. Rev. Lett.* **34**, 905 (1975); P. Mazur, *J. Phys. A* **15**, 3173 (1982).
 - [3] N. Straumann, *Class. Quantum Grav.* **16**, S155 (1993); P. Bizon, *Acta Phys. Pol. B* **25**, 877 (1994).
 - [4] B. Kleihaus and J. Kunz, *Phys. Rev. Lett.* **79**, 1595 (1997).
 - [5] S. A. Ridgway and E. J. Weinberg, *Phys. Rev. D* **52**, 3440 (1995).
 - [6] O. Brodbeck, M. Heusler, N. Straumann, and M. S. Volkov, *Phys. Rev. Lett.* **79**, 4310 (1997).
 - [7] M. S. Volkov and N. Straumann, *Phys. Rev. Lett.* **79**, 1428 (1997); O. Brodbeck and M. Heusler, *Phys. Rev. D* **56**, 6278 (1997).
 - [8] B. Kleihaus and J. Kunz, *Phys. Rev. Lett.* **78**, 2527 (1997).
 - [9] B. Kleihaus and J. Kunz, *Phys. Rev. D* **57**, 894 (1998).
 - [10] R. Bartnik and J. McKinnon, *Phys. Rev. Lett.* **61**, 141 (1988).
 - [11] M. S. Volkov and D. V. Gal'tsov, *Sov. J. Nucl. Phys.* **51**, 747 (1990); P. Bizon, *Phys. Rev. Lett.* **64**, 2844 (1990); H. P. Künzle and A. K. M. Masoud-ul-Alam, *J. Math. Phys.* **31**, 928 (1990).
 - [12] E. E. Donets and D. V. Gal'tsov, *Phys. Lett. B* **302**, 411 (1993); G. Lavrelashvili and D. Maison, *Nucl. Phys.* **B410**, 407 (1993).
 - [13] G. W. Gibbons and K. Maeda, *Nucl. Phys.* **B298**, 741 (1988); D. Garfinkle, G. T. Horowitz, and A. Strominger, *Phys. Rev. D* **43**, 3140 (1991).
 - [14] See, e.g., D. Kramer, H. Stephani, E. Herlt, and M. MacCallum, *Exact Solutions of Einstein's Field Equations* (Cambridge University Press, Cambridge, England, 1980), Chap. 17.
 - [15] C. Rebbi and P. Rossi, *Phys. Rev. D* **22**, 2010 (1980).
 - [16] B. Kleihaus and J. Kunz, *Phys. Lett. B* **329**, 61 (1994); B. Kleihaus and J. Kunz, *Phys. Rev. D* **50**, 5343 (1994).
 - [17] B. Kleihaus and J. Kunz, *Phys. Lett. B* **392**, 135 (1997).
 - [18] B. Kleihaus, J. Kunz and Y. Brihaye, *Phys. Lett. B* **273**, 100 (1991); J. Kunz, B. Kleihaus, and Y. Brihaye, *Phys. Rev. D* **46**, 3587 (1992).
 - [19] Y. Brihaye and J. Kunz, *Phys. Rev. D* **50**, 4175 (1994).
 - [20] The horizon of the axially symmetric Kerr solution in Boyer-Lindquist coordinates also resides at a surface of constant r .
 - [21] S. Weinberg, *Gravitation and Cosmology* (Wiley, New York, 1972).
 - [22] R. M. Wald, *General Relativity* (University of Chicago Press, Chicago, 1984).
 - [23] B. Kleihaus, J. Kunz, and A. Sood, *Phys. Lett. B* **374**, 289

- (1996); Phys. Rev. D **54**, 5070 (1996).
- [24] J. A. Smoller and A. G. Wasserman, Commun. Math. Phys. **161**, 365 (1994); P. Breitenlohner, P. Forgacs, and D. Maison, *ibid.* **163**, 141 (1994); P. Breitenlohner and D. Maison, *ibid.* **171**, 685 (1995).
- [25] The mass of the limiting solutions in Schwarzschild-like coordinates is constant for $0 \leq \tilde{x}_H \leq 1$, $\mu=1$.
- [26] W. Schönauer and R. Weiss, J. Comput. Appl. Math. **27**, 279 (1989); M. Schauder, R. Weiss, and W. Schönauer, The CADSOL Program Package, Universität Karlsruhe, Interner Bericht Nr. 46/92 (1992).
- [27] N. Straumann and Z. H. Zhou, Phys. Lett. B **237**, 353 (1990); **243**, 33 (1990).
- [28] N. J. Hitchin, N. S. Manton, and M. K. Murray, Nonlinearity **8**, 661 (1995); C. J. Houghton and P. M. Sutcliffe, Commun. Math. Phys. **180**, 343 (1996); Nonlinearity **9**, 385 (1996).
- [29] E. Braaten, S. Townsend, and L. Carson, Phys. Lett. B **235**, 147 (1990); R. A. Battye and P. M. Sutcliffe, Phys. Rev. Lett. **79**, 363 (1997); C. J. Houghton, N. S. Manton, and P. M. Sutcliffe, Nucl. Phys. **B510**, 507 (1998).